Monthly Notices of the ROYAL ASTRONOMICAL SOCIETY

MNRAS **429,** 1001–1026 (2013) doi:10.1093/mnras/sts383

A high-resolution spectropolarimetric survey of Herbig Ae/Be stars – I. Observations and measurements★

E. Alecian,[1,2]† G. A. Wade,[2] C. Catala,[1] J. H. Grunhut,[2,3] J. D. Landstreet,[4,5] S. Bagnulo,[5] T. Böhm,[6,7] C. P. Folsom,[5] S. Marsden[8,9] and I. Waite[9]

[1]*LESIA-Observatoire de Paris, CNRS, UPMC Univ., Univ. Paris-Diderot, 5 place Jules Janssen, F-92195 Meudon Principal Cedex, France*
[2]*Department of Physics, Royal Military College of Canada, PO Box 17000, Stn Forces, Kingston K7K 7B4, Canada*
[3]*Department of Physics, Queen's University, Kingston, ON K7L3N6, Canada*
[4]*Department of Physics & Astronomy, University of Western Ontario, London N6A 3K7, Canada*
[5]*Armagh Observatory, College Hill, Armagh BT61 9DG*
[6]*Université de Toulouse, UPS-OMP, IRAP, Toulouse, France*
[7]*CNRS, IRAP, 14 avenue Edouard Belin, F-31400 Toulouse, France*
[8]*Centre for Astronomy, School of Engineering and Physical Sciences, James Cook University, Townsville 4811, Australia*
[9]*Faculty of Sciences, University of Southern Queensland, Toowoomba 4350, Australia*

Accepted 2012 November 9. Received 2012 November 9; in original form 2012 February 15

ABSTRACT

This is the first in a series of papers in which we describe and report the analysis of a large survey of Herbig Ae/Be stars in circular spectropolarimetry. Using the ESPaDOnS and Narval high-resolution spectropolarimeters at the Canada–France–Hawaii and Bernard Lyot Telescopes, respectively, we have acquired 132 circularly polarized spectra of 70 Herbig Ae/Be stars and Herbig candidates. The large majority of these spectra are characterized by a resolving power of about 65 000, and a spectral coverage from about 3700 Å to 1 μm. The peak signal-to-noise ratio per CCD pixel ranges from below 100 (for the faintest targets) to over 1000 (for the brightest). The observations were acquired with the primary aim of searching for magnetic fields in these objects. However, our spectra are suitable for a variety of other important measurements, including rotational properties, variability, binarity, chemical abundances, circumstellar environment conditions and structure, etc. In this paper, we describe the sample selection, the observations and their reduction, and the measurements that will comprise the basis of much of our following analysis. We describe the determination of fundamental parameters for each target. We detail the least-squares deconvolution (LSD) that we have applied to each of our spectra, including the selection, editing and tuning of the LSD line masks. We describe the fitting of the LSD Stokes *I* profiles using a multicomponent model that yields the rotationally broadened photospheric profile (providing the projected rotational velocity and radial velocity for each observation) as well as circumstellar emission and absorption components. Finally, we diagnose the longitudinal Zeeman effect via the measured circular polarization, and report the longitudinal magnetic field and Stokes *V* Zeeman signature detection probability. As an appendix, we provide a detailed review of each star observed.

Key words: binaries: spectroscopic – stars: early-type – stars: magnetic field – stars: pre-main-sequence.

1 INTRODUCTION

Herbig (1960) was the first to perform a systematic study of a certain class of stars that we call now Herbig Ae/Be (HAeBe) stars, and whose observational parameters are as follows:

(i) the spectral type is A or earlier, with emission lines;
(ii) the star lies in an obscured region of space;
(iii) the star illuminates fairly bright nebulosity in its immediate vicinity.

★ Based on observations obtained at the Canada–France–Hawaii Telescope (CFHT) which is operated by the National Research Council of Canada, the Institut National des Sciences de l'Univers of the Centre National de la Recherche Scientifique of France and the University of Hawaii.

† E-mail: evelyne.alecian@obspm.fr

Published by Oxford University Press on behalf of the Royal Astronomical Society

Herbig selected these characteristics following the observational properties of the lower mass counterparts of HAeBe stars – T Tauri stars – and built a list of 26 HAeBe stars satisfying these criteria. This list, as well as the Herbig characteristics, have been extended since this original study (e.g. Herbig & Bell 1988; Thé, de Winter & Perez 1994; Vieira et al. 2003), and we now know of more than a hundred HAeBe stars of spectral type earlier than F5. All of them do not necessarily show all Herbig characteristics, but all of them have infrared (IR) excess with an abnormal extinction law (compared to classical Be stars).

The characteristics enumerated above suggest that HAeBe stars are very young, still surrounded by dust and gas in an envelope or disc. However, it was the spectroscopic study of Ström et al. (1972) that brought the first solid evidence that Herbig Ae/Be stars are in the pre-main-sequence (PMS) phase of quasi-static contraction, by showing that their surface gravities are systematically lower than those of their main-sequence (MS) counterparts. Herbig Ae/Be stars are therefore generally believed to be the evolutionary progenitors of MS intermediate-mass (A/B) stars.

Before the work of Palla & Stahler in the early 1990s, intermediate-mass stars with masses above 3 $M_{\odot}$ were believed to not experience a PMS phase similar to that of lower mass stars (Larson 1972). More detailed calculations performed by Palla & Stahler (1990, 1991, 1992, 1993), including deuterium burning during the protostellar collapse and the PMS phase, show that optically visible PMS stars could be observed, up to masses of about 8 $M_{\odot}$. There calculations considered a constant mass accretion rate during the protostellar collapse, and from the upper envelope of the distribution of Herbig Ae/Be stars in the Hertzsprung–Russell (HR) diagram, they concluded that all stars with masses lower than 8 $M_{\odot}$ are formed with a similar mass accretion rate of the order of $10^{-5}\,M_{\odot}\,yr^{-1}$.

However, following this work, many Herbig Be stars with masses larger than 8 $M_{\odot}$ have been discovered in the field of the Galaxy (see e.g. Fig. 4 of this paper), as well as in very young clusters (e.g. Martayan et al. 2008), implying that the simplified model of Palla & Stahler – with a constant mass accretion rate at all masses – may be insufficient to explain the observations. In fact, Palla & Stahler themselves proposed that the mass accretion rate should be time dependent. Norberg & Maeder (2000, hereafter NM00), and then Behrend & Maeder (2001, hereafter BM01), proposed that the mass accretion rate depends on the mass or the luminosity of the growing star. As a result, the mass accretion rate should increase while the star is growing and gaining in mass and luminosity, until the circumstellar (CS) matter becomes sufficiently rare and the massive accretion phase stops. Whereas a unique accretion rate of $10^{-5}\,M_{\odot}\,yr^{-1}$ as proposed by Palla & Stahler (1993) results in a maximum PMS star mass of around 8 $M_{\odot}$, a modulated mass accretion rate, as proposed by NM00 and BM01, allows the birthline to reach the zero-age main sequence (ZAMS) at much higher masses (above 20 $M_{\odot}$).

Herbig Ae/Be stars are indeed observed with masses as large as 20 $M_{\odot}$, with a distribution more concentrated between 1.5 and 3 $M_{\odot}$ (see Table 2 and Fig. 4 of this paper). Their spectral types are found between F5 and B2 (Vieira et al. 2003), and many of them show some spectroscopic and photometric activity, reflective of their young age. Many types of activity can be found among Herbig Ae/Be stars, but their origins are not well understood. Among them we find the UX Ori stars, with the Herbig Ae star UX Ori as the prototype. These stars are characterized by a very strong photometric variability (up to 3 mag in the *V* band), and by the presence of transient absorption features in their spectra that may be due to episodic accretion events (e.g. Mora et al. 2002). While some authors think that these characteristics are created by the infall of cometary bodies on to the star (e.g. Grady et al. 2000b), others are more convinced by the theory of accretion from a disc, whether via the intermediary of a magnetic field, or not (Natta, Grinin & Tambovtseva 2000; Mora et al. 2004). The presence of winds is detected in many HAeBe stars through P Cygni profiles observed in Hα and sometimes in metallic and He lines (e.g. Finkenzeller & Mundt 1984; Bouret, Catala & Simon 1997; Bouret & Catala 1998). Some authors have proposed that these winds have a stellar origin (e.g. Böhm & Catala 1994), while others believe that a disc wind is present (e.g. Corcoran & Ray 1998; Vieira et al. 2003). However, strong variability in Hα emission profiles is observed in a few HAeBe stars, some of them at times showing double-peaked profiles, and sometimes P Cygni profiles (e.g. Thé et al. 1985a; Catala et al. 1986a). These stars show periodic cyclical modulations not only of their Hα emission, but also of metallic lines such as the ultraviolet (UV) Mg II h&k doublet (e.g. Catala et al. 1989), as well as of their X-ray emission (e.g. Testa et al. 2008). Their spectra also show UV emission lines of highly ionized species such as N V and O VI (e.g. Bouret et al. 1997). Bouret et al. (1997) proposed that these characteristics are due to the presence of a non-axisymmetric wind controlled by a stellar magnetic field. Various non-photospheric spectral features, in addition to those discussed above, are observed in the spectra of HAeBe stars, some with variability and others without. However, the interpretation of each one of these features, as well as their diversity, is not understood at all. The fact that HAeBe stars cover such a large range of mass, temperatures, age and evolutionary state, as well as the fact that these stars evolve at a variety of rates, certainly must be connected with the large variety of observed HAeBe activity phenomena and our difficulties to interpret them.

HAeBe stars are important astrophysical objects because they represent the late formative stages of intermediate-mass stars. They are therefore significant for understanding general and specific phenomena involved in star formation. Moreover, HAeBe stars can help us to understand a number of perplexing properties of their MS descendants, in particular chemical peculiarities, very slow rotation and magnetic fields, observed individually or in combination in a significant fraction of MS A/B stars.

Among the MS A/B stars, a significant fraction shows photospheric abundance anomalies (as compared to solar abundances, and to the abundances of the majority of MS A/B stars). These anomalies are believed to result from atomic diffusion within their surface layers due to the competition between radiative levitation and gravitational settling (e.g. Michaud 1970). One important condition necessary to allow this phenomenon to occur is the absence of strong deep mixing in those layers, which would tend to overwhelm these separation processes. As rotation-driven circulation is an important source of such mixing, this condition implies that such chemically peculiar stars should be slow rotators. It has been observed that nearly all chemically peculiar Am, Ap/Bp and HgMn stars are characterized by slow rotation (rotation periods longer than ~1 d) compared to the 'normal' (non-peculiar) A/B stars (Abt & Morrell 1995). The origin of this slow rotation is not well understood. In the case of Am and HgMn stars, slow rotation might be the result of tidal interaction occurring in close binary systems (i.e. those with orbital periods shorter than 100 d; e.g. Abt 2009). The mechanism responsible for the slow rotation of Ap/Bp stars is likely related to their strong magnetic fields. Stępień (2000) discussed different theories aimed at explaining this slow rotation, and he concluded that magnetic braking must occur during the PMS phase in order to reproduce the rotational angular momenta of MS

A/B stars. Stepien demonstrated that magnetic coupling of a PMS star with its accretion disc would slow the rotation of the star and increase its rotation period to a few days. In order to produce the slowest rotators – those with observed rotation periods greater than about one month – the disc must disappear sufficiently early during the PMS phase to allow strong magnetized winds to carry away a large quantity of angular momentum before the star reaches the ZAMS.

Until recently we had very few observational constraints on the magnetic fields and the rotation of Herbig Ae/Be stars. To our knowledge, only two thorough observational studies of the evolution of the angular momentum of intermediate-mass stars during the PMS phase have been undertaken. Böhm & Catala (1995) concluded that if these stars rotate as solid bodies, the evolution of the angular momentum must depend on stellar mass, while if the internal rotation varies as (radius)$^{-2}$, the observations of HAeBe and MS A/B stars in young clusters are consistent with conservation of total angular momentum at all masses. Wolff, Strom & Hillenbrand (2004) concluded that PMS intermediate-mass stars lose angular momentum before they start the PMS phase, while angular momentum is conserved during the radiative phase of PMS evolution. Both of these analyses provided very interesting results that should be discussed in the framework of a scenario of angular momentum evolution that includes magnetic fields.

A number of studies have been attempted to detect magnetic fields in Herbig Ae/Be stars, without much success (e.g. Catala et al. 1993; Hubrig, Schöller & Yudin 2004). Apart from a marginal detection in HD 104237 reported by Donati et al. (1997), and a possible detection in HD 101412 proposed by Wade et al. (2007) (both being now firmly confirmed magnetic stars: Alecian et al., in preparation), no other convincing magnetic detections have been reported before the present survey. The reason is likely limited precision and an insufficiently large stellar sample as a consequence of limited observational capabilities. Fortunately, many of these limitations are overcome by today's spectropolarimetric facilities: telescopes with large collecting area, high-efficiency instruments, large spectral range and high spectral resolution.

In order to thoroughly investigate magnetism and rotation in HAeBe stars, we have performed a large survey of 70 stars using the newest high-resolution spectropolarimetric instruments: ESPaDOnS [at the Canada–France–Hawaii Telescope (CFHT), USA] and Narval (at the Télescope Bernard Lyot, TBL, France). Within the context of this survey we have detected a small number of new magnetic stars and confirmed the presence of a magnetic field already discovered during a parallel ESPaDOnS programme focused on massive stars in Orion (LP Ori; Petit et al. 2008). Those discoveries (HD 190073, HD 200775, HD 72106, V380 Ori and LP Ori), and the analysis we performed to characterize their magnetic fields and related properties, have already or will be described in other papers (Wade et al. 2005; Catala et al. 2007; Alecian et al. 2008a; Folsom et al. 2008; Petit et al. 2008; Alecian et al. 2009b; Petit et al., in preparation). While this survey is focusing on HAeBe stars in the field of the Galaxy, we have also performed a similar survey of HAeBe stars in three young clusters and detected three more magnetic stars: NGC 6611 601, NGC 2244 201 and NGC 2264 83 (Alecian et al. 2008b, 2009a). The description of this cluster survey will be presented in an upcoming paper (Alecian et al., in preparation).

We are now publishing a series of papers describing the complete sample of observed field stars, discussing the observations and their analysis (this paper, which is Paper I of the series), an analysis of their rotation velocities (Alecian et al. 2013, hereafter Paper II), an analysis of their magnetic properties (Wade et al., in preparation, hereafter Paper III), and the characterization of the CS contributions to the spectra of the sample (Alecian et al., in preparation, hereafter Paper IV).

This paper is organized as follows. In Section 2 we review the sample selection, and in Section 3 the observational procedure and data reduction, and summarize the characteristics and quality of the reduced spectra. In Section 4 we determine fundamental parameters for the stars of the sample, and in Section 5 we describe the extraction and fitting of the least-squares deconvolution (LSD) profiles that we use for the majority of our analysis. In Section 6 we discuss the magnetic field diagnosis carried out in a number of different ways. Section 7 provides a discussion of the results and conclusions relevant to the analysis to be reported in Papers II, III and IV.

2 SAMPLE SELECTION

Our study required the selection of a relatively large number of HAeBe stars to allow us to derive statistically meaningful conclusions about the presence of magnetic fields in these stars. Various literature sources were used for target selection, primarily the catalogues of HAeBe stars and HAeBe candidates by Thé et al. (1994) and Vieira et al. (2003).

The catalogue of Thé et al. (1994) contains six categories of stars; the stars selected for our study were obtained only from the first category, which contains stars historically known as HAeBe stars, or strong candidates of the group. According to the authors, all of these stars possess near- or far-IR excess and emission lines, associated with the presence of CS dust, discs and energetic outflows which are usually found in HAeBe stellar environments. On the other hand, Vieira et al. (2003) produced a catalogue of HAeBe stars and probable candidates from an initial search for new T Tauri stars (PMS stars of lower mass) using the *Infrared Astronomical Satellite* (*IRAS*) point source catalogue.[1] Because the initial search was based on CS dust properties, it included HAeBe stars along with T Tauri stars. Vieira et al. extracted the HAeBe stars by filtering the data using specific requirements such as a spectral type earlier than F5, emission at Hα and a minimum level of IR emission. The majority of the stars were associated by the authors with a star-forming region. Based on the quality of these two literature sources and the arguments presented by their authors, we conclude that all of the stars in our sample are *bona fide* HAeBe stars. In total, 70 HAeBe stars have been selected with visual magnitudes lower than 12, spanning in spectral type from F5 to B0.

Measurements with high-resolution spectropolarimeters (such as ESPaDOnS@CFHT or Narval@TBL) have a high enough resolving power to take advantage of the information contained in the line profiles of metallic lines, as has already been demonstrated in earlier studies with the MuSiCoS spectropolarimeter (e.g. Wade et al. 2000; Petit et al. 2004). ESPaDOnS magnetic field measurements have standard errors which decrease strongly with decreasing $v \sin i$ and with increasing richness and strength of the metallic line spectrum (cf. Landstreet 1982; Shorlin et al. 2002). To fully exploit this dependence, and thus to obtain the most precise measurements possible, we have preferentially selected our targets for low $v \sin i$ ($\lesssim$100 km s^{-1}) where available $v \sin i$ data allowed us to perform such a selection. However, because accurate measurements of $v \sin i$ are not available for many HAeBe stars, a significant fraction of our targets (about one-third) turn out to be relatively rapid rotators.

[1] http://irsa.ipac.caltech.edu/

3 OBSERVATIONS AND DATA REDUCTION

The 132 program star observations reported here were obtained between 2004 and 2010 using two high-resolution spectropolarimeters: the ESPaDOnS spectropolarimeter at the CFHT (80 spectra), and the Narval spectropolarimeter at the Télescope Bernard Lyot (52 spectra). The ESPaDOnS observations were obtained during six observing runs in 2004 (technical and commissioning runs), 2005 and 2006 (competitively allocated PI time), including the first scientific ESPaDOnS run. The Narval observations were obtained during seven observing runs between 2007 and 2010 (competitively allocated PI time).

The basic technical characteristics of ESPaDOnS and Narval are nearly identical. The polarization analysis unit is located at the Cassegrain focus of the telescope. The stellar image is formed on an aperture followed by a collimating lens. The beam then passes through a rotatable $\lambda/2$ retarder, a fixed $\lambda/4$ retarder, a second rotatable $\lambda/2$ retarder and finally a small-angle Wollaston prism, followed by a lens which refocuses the (now double) star image on the inputs of two optical fibres. This relatively complex polarization analyser is necessary because one of the fundamental design parameters for ESPaDOnS/Narval was very wide wavelength coverage (approximately 3700 Å to 1.04 μm). To have retarders which are approximately achromatic over this wide range, ESPaDOnS uses Fresnel rhombs. A single Fresnel rhomb acts as a $\lambda/4$ retarder, but deviates the beam, while two Fresnel rhombs in series form a $\lambda/2$ plate without beam deviation. To minimize mechanical complications, only the double (non-deviating) Fresnel rhombs are allowed to rotate; the configuration chosen is the minimum which allows one to analyse all of the Stokes polarization components (Q, U, V) by appropriate orientation of the axes of the successive retarders.

The two output beams from the Wollaston prism, which have been split into the two components of circular polarization (for this study) by appropriate retarder orientations, are then carried by the pair of optical fibres to a stationary and temperature-controlled cross-dispersed spectrograph where two interleaved spectra are formed, covering virtually the entire desired wavelength range with a resolving power of $R \simeq 65\,000$. The I component of the stellar Stokes vector is formed by adding the two corresponding spectra, while the desired polarization component (Q, U, V) is obtained essentially from the difference of the two spectra. To minimize systematic errors due to small misalignments, differences in transmission, effects of seeing, etc., one complete observation of a star consists of four successive subexposures; for the second and third, the retarder orientations are changed so as to exchange the beam paths of the two analysed spectra (see Donati et al. 1997).

The actual reduction of observations is carried out at the observatory using the dedicated software package LIBRE-ESPRIT. LIBRE-ESPRIT subtracts bias, locates the various spectral orders on the CCD image, measures the shape of each order and models the (varying) slit geometry, identifies comparison lines for each order and computes a global wavelength model of all orders, performs an optimal extraction of each order, and combines the resulting spectra to obtain 1D intensity (Stokes I) and circular polarization (Stokes V) spectra. The Stokes V spectrum normally has the continuum polarization removed, as this arises mainly from instrumental effects and carries little information about the star. Each spectrum is corrected to the heliocentric frame of reference, and may optionally be divided by a flat-field and be approximately normalized (see Donati et al. 1997, and ESPaDOnS webpages[2]). Due to the presence of strong emission lines in the spectra of many of our targets, the automatic LIBRE-ESPRIT normalization fails to achieve a satisfactory rectification of the continuum. We have therefore turned off this option in LIBRE-ESPRIT, and normalized the final reduced 1D spectra manually, order by order.

Diagnostic null spectra called N spectra, computed by combining the four successive subexposures of polarization in such a way as to have the real polarization cancelled out (Donati et al. 1997), are also calculated by LIBRE-ESPRIT. The N spectra test the system for spurious polarization signals. In all of our observations, the N spectra are quite featureless, as expected. The final spectra consist of ASCII files tabulating I/I_c, V/I_c, N/I_c, and estimated uncertainty per pixel as a function of wavelength, order by order.

The log of spectropolarimetric observations is reported in Table 1. The 132 observations include 112 observations of 64 apparently non-magnetic program stars, nine observations of five magnetic program stars (the discovery and/or confirmation observations of each) and 11 observations of one possibly newly detected magnetic program star (HD 35929).

Because the program stars observed in this study are characterized by a large range of visual magnitudes (reflecting their diverse luminosities, distances and extinctions due to their surrounding environments), the distribution of their apparent magnitudes m_V (shown in Fig. 1, left-hand panel) is rather broad (with a mean of 8.9, a minimum of 4.2 and a maximum of 11.9). As a consequence, our data yield a broad distribution of signal-to-noise ratios (S/N values, illustrated inFig. 1, right-hand panel), ranging from below 100 per CCD pixel to over 1000.

4 FUNDAMENTAL PARAMETERS

4.1 Effective temperature and surface gravity determination

The temperature and gravity, as well as their errors, of each star was first taken from the literature, and has then been compared to our data as follows. For effective temperatures below 15 000 K, we have calculated synthetic spectra in the local thermodynamic equilibrium (LTE) approximation, using the code SYNTH of Piskunov (1992). SYNTH requires, as input, atmosphere models, obtained using the ATLAS 9 program (Kurucz 1993), and a list of spectral line data obtained from the Vienna Atomic Line Database[3] (VALD; Piskunov et al. 1995; Kupka et al. 1999; Ryabchikova et al. 1999). Above 15 000 K we used TLUSTY non-LTE atmosphere models and the SYNSPEC code (Hubeny 1988; Hubeny & Lanz 1992, 1995), to calculate synthetic spectra. At all temperatures the synthetic spectra have been computed with a solar metallicity (see Section 4.2). Then we compared, by eye, the observed to the synthetic spectra, and if necessary adjusted the temperature (holding $\log g = 4.0$ constant) until a best fit was achieved. For some stars, the temperatures found in the literature were not able to reproduce our spectra, and therefore we give here new determinations of $T_{\rm eff}$.

In this procedure we fixed the surface gravity $\log g = 4.0$ because for most of the stars of our sample, the determination of $\log g$ using our data is not possible for the following reasons. First, the continuum level is very difficult to determine in echelle spectra and most of the Balmer lines are spread over two orders, making the determination of $\log g$ from the wings of the Balmer lines very

[2] http://www.cfht.hawaii.edu/Instruments/Spectroscopy/Espadons
[3] http://ams.astro.univie.ac.at/∼vald/

Table 1. Log of observations of the HAeBe program stars. Columns 1 and 2 give the designations of the stars. The date, Universal Time (UT) and Heliocentric Julian Date (HJD) of the start of the observation are given in columns 3 and 4. The total exposure time is given in column 5. Column 6 gives the peak S/N per CCD pixel at the wavelength indicated in column 7. Columns 8–11 give the number of lines used to compute the LSD profiles with the full and cleaned masks and the S/N in the LSD *V* profile. The final column indicates the instrument associated with the observation.

							Full mask		Cleaned mask		
HD or BD number	Other name	Date (dd/mm/yy) UT time	HJD − 245 0000	Total exp. time (s)	Peak S/N	λ (nm)	No. of LSD lines	LSD S/N	No. of LSD lines	LSD S/N	Instrument
BD−06 1259	BF Ori	21/02/05 09:17	3422.88915	4800	192	515	2401	1986	466	1426	ESPaDOnS
		12/03/09 19:41	4903.32074	4640	83	567	2398	3224	397	874	Narval
		12/03/09 21:03	4903.37805	4640	88	731					Narval
BD−06 1253	V380 Ori	20/02/05 09:32	3421.90001	4800	144	781					ESPaDOnS
BD−05 1329	T Ori	24/08/05 14:53	3607.11832	3600	245	731	1487	2890	662	2201	ESPaDOnS
BD−05 1324	NV Ori	12/01/06 04:56	3747.71083	3200	163	708	5896	2759	368	860	ESPaDOnS
BD+41 3731		26/08/05 09:03	3608.88285	4000	309	527	362	1564	320	2552	ESPaDOnS
		06/11/07 21:54	4411.41380	5800	178	552	382	2675	310	1444	Narval
BD+46 3471	V1578 Cyg	26/08/05 10:59	3608.96354	4800	304	708	1274	3540	586	2811	ESPaDOnS
BD+61 154	V594 Cas	22/02/05 05:56	3423.74367	3600	144	730	550	1332	12	148	ESPaDOnS
		24/08/05 11:01	3606.96314	5600	208	515	570	870	12	355	ESPaDOnS
BD+65 1637	V361 Cep	11/06/06 14:49	3898.11845	2400	237	730	371	1728	86	738	ESPaDOnS
		24/09/09 21:43	5099.40934	8400	276	731	343	2151	73	911	Narval
BD+72 1031	SV Cep	12/06/06 15:00	3899.12535	1600	159	730	967	1547	561	1301	ESPaDOnS
		11/11/07 21:46	4416.40939	6400	139	731	1025	1394	543	1228	Narval
HD 9672	49 Cet	25/08/05 11:40	3607.98968	800	910	515	2079	17 572	2079	17572	ESPaDOnS
HD 17081	π Cet	20/02/05 05:29	3421.72749	480	925	515	518	8006	234	4885	ESPaDOnS
		21/02/05 05:31	3422.72864	480	1049	515	517	9158	234	5837	ESPaDOnS
HD 31293	AB Aur						1525	5293	590	6641	ESPaDOnS
		20/02/05 05:53	3421.74513	1200	395	527	1536	8391	559	3500	ESPaDOnS
		22/02/05 08:26	3423.85121	2400	547	527	1604	9895	559	5575	ESPaDOnS
HD 31648	MWC 480	22/02/05 09:13	3423.88401	2400	389	527	3411	9335	1073	6583	ESPaDOnS
		25/08/05 12:45	3608.03208	2000	435	708	3420	9671	1067	6934	ESPaDOnS
HD 34282		25/08/05 13:57	3608.07957	4000	246	708	2924	4904	2924	4904	ESPaDOnS
HD 35187 B		26/08/05 13:13	3609.05072	2000	360	708	2104	5967	1383	5466	ESPaDOnS
HD 35929		13/11/07 00:50	4417.53905	4000	415	566	4853	12 302	3055	10076	Narval
		14/11/07 00:29	4418.52488	2000	213	708	4962	11 800	3050	4999	Narval
		20/02/09 19:33	4883.31686	2000	335	731	4951	5830	3010	14214	Narval
		20/02/09 20:12	4883.34386	2000	341	731					Narval
		20/02/09 20:49	4883.36939	2000	323	731					Narval
		21/02/09 19:13	4884.30273	2000	309	731	4852	16 589	3007	12287	Narval
		21/02/09 19:49	4884.32826	2000	298	731					Narval
		21/02/09 20:26	4884.35380	2000	281	731					Narval
		11/03/09 19:31	4902.31377	2000	284	731	4851	14 318	3006	10574	Narval
		11/03/09 20:08	4902.33930	2000	250	731					Narval
		11/03/09 20:44	4902.36482	2000	265	731					Narval
HD 36112	MWC 758						3758	7123	284	2792	ESPaDOnS
		20/02/05 06:30	3421.77182	2400	322	708	4185	9217	271	2236	ESPaDOnS
HD 36910	CQ Tau	04/04/08 20:12	4561.33902	6000	198	731	5671	5037	1219	3209	Narval
HD 36917	V372 Ori	08/11/07 23:48	4413.49636	4000	208	552	1064	2477	1064	2477	Narval
HD 36982	LP Ori	09/11/07 01:05	4413.54984	4000	136	552	614	3430	187	937	Narval
		10/11/07 00:56	4414.54299	6000	306	552	615	3270	187	2178	Narval
		11/11/07 00:03	4415.50631	4400	264	552	609	4838	187	2088	Narval
		11/11/07 01:21	4415.56085	4400	314	552					Narval
		12/11/07 01:05	4416.54958	6000	426	552	579	1447	187	3091	Narval
HD 37258	V586 Ori	24/02/09 19:15	4887.30404	6600	292	553	1872	5262	559	3215	Narval
HD 37357		24/02/09 22:15	4887.42954	4440	270	553	1965	4795	723	3550	Narval
HD 37806	MWC 120	25/08/05 15:10	3608.13042	2000	468	515	577	4293	53	1793	ESPaDOnS
HD 38120		13/03/09 22:23	4904.43316	3600	230	553	1400	3152	1436	3021	Narval
HD 38238	V351 Ori	16/03/07 20:16	4176.34501	4680	247	731	4790	6822	3356	6190	Narval
HD 50083	V742 Mon	13/11/07 01:50	4417.57965	2000	487	553	584	5699	157	2508	Narval
		03/04/08 20:58	4560.37363	2000	500	553	628	7080	147	2287	Narval
HD 52721		07/11/07 03:33	4411.65007	2000	523	553	628	5350	273	4090	Narval
		03/04/08 20:14	4560.34420	2000	467	553	662	6253	250	3590	Narval
HD 53367		20/02/05 10:31	3421.94295	1200	363	708	545	2646	59	977	ESPaDOnS
		21/02/05 10:25	3422.93832	2400	505	566	548	4289	59	1621	ESPaDOnS
HD 68695		22/02/05 10:53	3423.95853	2400	128	527	1550	1579	1550	1575	ESPaDOnS
HD 72106		22/02/05 10:04	3423.92478	2400	236	515					ESPaDOnS
HD 76534 A		22/02/05 11:40	3423.99189	1800	221	708	436	1578	11	353	ESPaDOnS

Table 1 – *continued*

HD or BD number	Other name	Date (dd/mm/yy) UT time	HJD − 245 0000	Total exp. time (s)	Peak S/N	λ (nm)	Full mask: No. of LSD lines	Full mask: LSD S/N	Cleaned mask: No. of LSD lines	Cleaned mask: LSD S/N	Instrument
HD 98922		21/02/05 11:54	3423.00115	1600	451	527	683	3089	578	2872	ESPaDOnS
HD 114981	V958 Cen	20/02/05 12:13	3422.01396	1600	329	515	518	6680	210	1756	ESPaDOnS
		12/01/06 15:01	3748.12665	2400	633	515	531	3018	211	4060	ESPaDOnS
HD 135344		10/01/06 15:40	3746.15200	2400	128	731	6631	2555	6631	2555	ESPaDOnS
HD 139614		20/02/05 13:50	3422.07904	3600	298	708	3495	5853	7023	9542	ESPaDOnS
		21/02/05 13:46	3423.07633	2800	274	708	3519	5587	7004	9242	ESPaDOnS
		22/02/05 14:14	3424.09588	2400	294	708	3513	6592	7020	10579	ESPaDOnS
HD 141569		13/02/06 12:29	3780.02056	4000	301	708	1496	2821	1418	2723	ESPaDOnS
		07/03/07 13:20	4167.05806	5400	1053	566	1478	16 345	1395	15985	ESPaDOnS
HD 142666	V1026 Sco	20/02/05 12:54	3422.03917	2400	237	708	3855	4123	2496	3711	ESPaDOnS
		22/02/05 13:16	3424.05441	3600	338	708	3885	7184	2549	6402	ESPaDOnS
		22/05/05 07:50	3512.83235	3600	292	708	3866	6005	2543	5381	ESPaDOnS
		22/05/05 08:55	3512.87760	3600	293	708	3867	5141	2506	5365	ESPaDOnS
		23/05/05 08:25	3513.85638	3600	256	708	3920	6425	2507	4593	ESPaDOnS
		24/05/05 07:54	3514.83487	3600	308	708	3893	5863	2530	5725	ESPaDOnS
		25/05/05 08:02	3515.84083	3600	282	708	4775	7989	2507	5209	ESPaDOnS
HD 144432		20/02/05 14:47	3422.11732	2400	323	708	4792	9430	1751	5893	ESPaDOnS
		21/02/05 14:46	3423.11688	3200	368	708	3426	12 788	1742	7118	ESPaDOnS
HD 144668	HR 5999	24/08/05 05:38	3606.73345	1200	569	708	3863	8503	2821	12340	ESPaDOnS
HD 145718	V718 Sco	26/08/05 05:32	3608.72972	2800	403	730	1760	6149	2284	7274	ESPaDOnS
HD 150193	V2307 Oph	24/08/05 06:20	3606.76406	2800	453	730	1768	9845	1541	6043	ESPaDOnS
HD 152404	AK Sco	15/02/06 14:46	3782.11538	3600	393	708	6684	10 308	2634	7454	ESPaDOnS
HD 163296		22/05/05 09:54	3512.91769	2400	588	527	1764	7008	1123	8391	ESPaDOnS
		23/05/05 10:02	3513.92318	3600	460	515	1801	10 426	1112	5924	ESPaDOnS
		24/05/05 09:49	3514.91391	3600	615	515	1798	7439	1157	8981	ESPaDOnS
		24/05/05 14:48	3515.12170	2400	448	515	1714	3678	1121	6362	ESPaDOnS
		25/05/05 09:52	3515.91662	3600	617	527	1791	10 394	1097	8744	ESPaDOnS
		25/05/05 14:53	3516.12540	2400	436	566	1753	11 221	1056	6092	ESPaDOnS
		25/08/05 05:39	3607.73704	1200	641	515	5421	6488	1104	9561	ESPaDOnS
HD 169142		20/02/05 15:34	3422.14750	2400	270	708	5450	5421	3718	5865	ESPaDOnS
		22/02/05 15:01	3424.12494	2400	208	708	5502	8648	3788	4861	ESPaDOnS
		22/05/05 10:41	3512.95012	2400	311	708	5479	14 187	3737	7728	ESPaDOnS
		24/08/05 07:10	3606.80061	2000	473	708	554	1926	3751	12614	ESPaDOnS
HD 174571	MWC 610	17/03/07 03:51	4176.65909	3600	283	731	586	2557	343	2086	Narval
		16/04/08 02:35	4572.60859	3900	245	731	626	5359	342	1621	Narval
HD 176386		25/08/05 06:09	3607.75872	1600	573	708	820	9459	601	5297	ESPaDOnS
HD 179218		21/02/05 15:30	3423.14213	1200	298	527	849	2949	271	2117	ESPaDOnS
		26/08/05 08:10	3608.84465	1600	631	515	841	6965	271	4945	ESPaDOnS
		03/10/09 20:53	5108.37217	7200	866	553	1768	5059	255	6667	Narval
HD 190073	V1295 Aql	22/05/05 11:40	3512.98887	3290	411	527					ESPaDOnS
HD 200775	MWC 361	22/05/05 14:35	3513.10716	3600	555	731					ESPaDOnS
HD 203024		24/08/05 09:38	3606.90562	2800	365	515	1765	5954	1238	5567	ESPaDOnS
		07/11/07 22:17	4412.43070	4800	307	552	1799	2353	1238	4811	Narval
HD 216629	IL Cep	10/06/06 15:06	3897.12935	1200	301	730	437	1773	90	910	ESPaDOnS
		08/12/06 07:09	4077.79899	1200	227	708	438	2115	81	758	ESPaDOnS
		05/11/07 21:18	4410.39095	5700	339	731	2871	3856	90	1112	Narval
HD 244314	V1409 Ori	05/11/07 23:19	4410.47647	6000	158	552	3449	7804	1799	2363	Narval
HD 244604	V1410 Ori	24/08/05 13:47	3607.07333	3600	329	527	1736	2631	2016	6964	ESPaDOnS
HD 245185	V1271 Ori	20/02/05 07:39	3421.82069	4800	192	515	1971	2213	1736	2631	ESPaDOnS
HD 249879		05/04/08 21:03	4562.37504	6000	133	553	492	1726	982	1951	Narval
HD 250550	V1307 Ori	08/11/07 00:23	4412.52023	5360	202	553	416	2282	387	1403	Narval
HD 259431	V700 Mon	17/03/07 22:40	4177.44524	5100	302	731	402	1528	261	1583	Narval
		24/02/09 23:31	4887.48247	2400	274	731	404	2078	253	1473	Narval
		17/03/10 20:23	5273.35057	2400	199	731	1100	1072	258	1178	Narval
HD 275877	XY Per	11/12/06 06:24	4080.77111	3600	348	708	2897	6912	453	3058	ESPaDOnS
		25/09/09 00:46	5099.53643	7200	299	731	2715	5390	412	2419	Narval
HD 278937	IP Per	21/02/05 06:26	3422.76644	4800	195	666	2892	3084	2871	3856	ESPaDOnS
		21/02/05 07:50	3422.82473	4800	171	527	2924	2735	2892	3084	ESPaDOnS
		22/02/05 07:14	3423.79948	4800	172	708	395	30 034	2924	2735	ESPaDOnS
HD 287823		17/03/07 21:16	4177.38573	3120	112	552	3671	2836	1100	1072	Narval
HD 287841	V346 Ori	20/02/09 22:23	4883.43440	7740	151	731	2112	2979	3671	2836	Narval
HD 290409		07/11/07 00:17	4411.51658	6000	171	552	1983	1315	2112	2979	Narval

Table 1 – *continued*

HD or BD number	Other name	Date (dd/mm/yy) UT time	HJD − 245 0000	Total exp. time (s)	Peak S/N	λ (nm)	Full mask No. of LSD lines	Full mask LSD S/N	Cleaned mask No. of LSD lines	Cleaned mask LSD S/N	Instrument
HD 290500		21/02/09 21:49	4884.41137	6180	92	731	484	2468	360	629	Narval
		21/02/09 23:38	4884.48650	6180	82	731					Narval
HD 290770		24/02/09 20:53	4887.37237	4200	280	553	423	2513	172	1878	Narval
HD 293782	UX Ori	11/01/06 04:55	3746.70929	3200	174	708	1521	2375	1521	2375	ESPaDOnS
HD 344361	WW Vul	24/08/05 08:20	3606.85206	5200	274	708	1477	2060	764	3036	ESPaDOnS
		06/11/07 18:59	4411.29021	6800	152	552	1502	3660	756	1763	Narval
	LkHa 215	15/04/08 20:49	4572.36556	6000	90	731	370	32 681	204	26607	Narval
		11/03/09 22:14	4902.42813	5820	176	731	615	1476	233	26231	Narval
	MWC 1080	25/08/05 08:10	3607.84527	6400	320	839					ESPaDOnS
	VV Ser	26/08/05 06:57	3608.79270	6400	241	809	491	1418	226	856	ESPaDOnS
	VX Cas	25/08/05 10:05	3607.92466	6400	146	515	1230	1499	1230	1499	ESPaDOnS

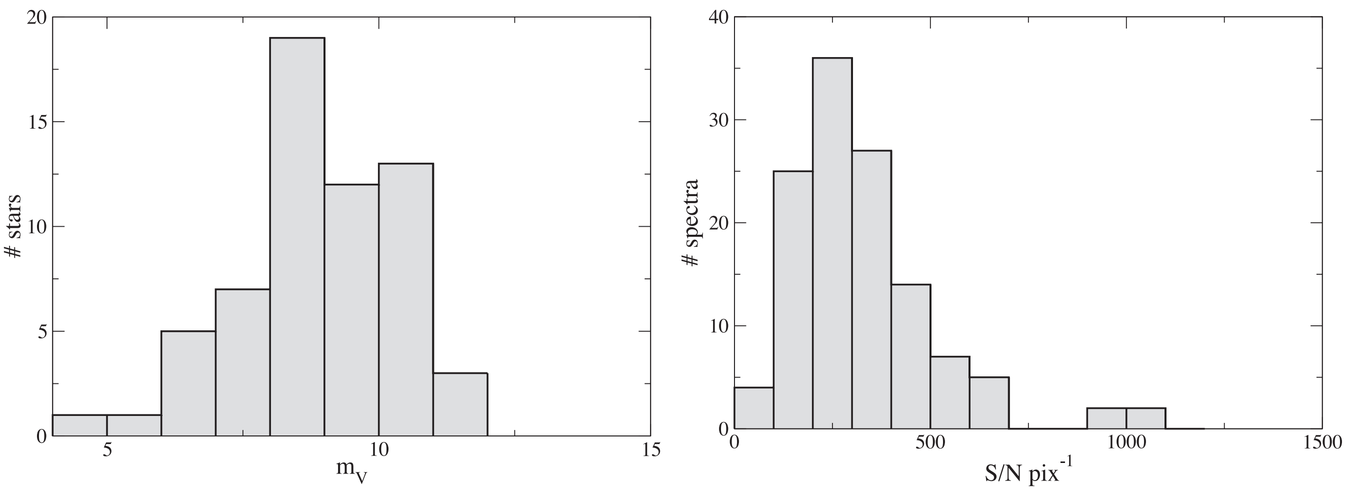

Figure 1. Distributions of m_V (left) and S/N (right) of the sample stars.

imprecise. Then, the spectra of many of our targets are heavily contaminated with CS emission/absorption and especially in the spectral lines of Fe, Ti, Si and Cr, which makes impossible the determination of surface gravity from the ionization equilibrium of abundant species. Typical values of $\log g$ in HAeBe stars comprise between 3.5 and 4.5 (e.g. Folsom et al. 2012). We have therefore adopted a value of 4.0 for all stars for which a determination from our observations was not possible.

For a few Herbig stars whose metallic spectral lines are only very faintly contaminated with CS emission/absorption, we obtained very high quality, high-resolution spectra. To determine accurate effective temperature and gravity in these few cases, we developed an automatic procedure, based on a comparison of the observed spectrum to a grid of model spectra. The grid is composed of LTE SYNTH3 models (Kochukhov 2007), computed using Kurucz's ATLAS 9 atmospheres. The models assume solar abundances and no macro-turbulence, while the grid varies the microturbulence between 0, 1, 2, 3, 4 and 5 km s^{-1}. The atomic line lists were extracted from VALD, for all lines with a predicted line depth greater than 0.01 times the continuum. The models in our grid range from an effective temperature of 6500 to 15 000 K, in steps of 100 K. In addition, the models range from 3.0 to 5.0 dex in $\log(g)$ in 0.5 dex steps. The rotational broadening and disc integration of the SYNTH3 models used for comparison with the observed spectra was carried out using the code S3DIV (Kochukhov 2007).

For this procedure the spectral region between 420 and 520 nm was modelled, as lines in this region show the strongest sensitivity to temperature variations for stars with temperatures within our grid range. We used a brute-force search for the lowest χ^2 by comparing the observation to each model within a pre-selected parameter space [corresponding to a pre-defined temperature range, a pre-defined range in $\log(g)$ and each value of microturbulence] of the grid. The initial search parameters were chosen based on photometric or spectroscopic literature estimates. For each model, we fit the $v \sin i$ to the observations using a χ^2 minimization routine as well. The Balmer line regions were ignored due to imprecise continuum normalization of the short echelle orders and strong local emission.

Once the best-fitting model was identified, we carried out a visual comparison between the model and the observation to determine which regions (if any) were poorly fitted, likely due to contamination from CS material. We then reran our spectrum fitting procedure with these regions ignored to improve our fits. If an observation showed strong emission in metallic lines, this procedure would not provide a realistic estimate on the stellar parameters. Examples demonstrating the quality of fit we are able to achieve, for both a low $v \sin i$ and a high $v \sin i$ star, are shown in Fig. 2. The parameters derived in

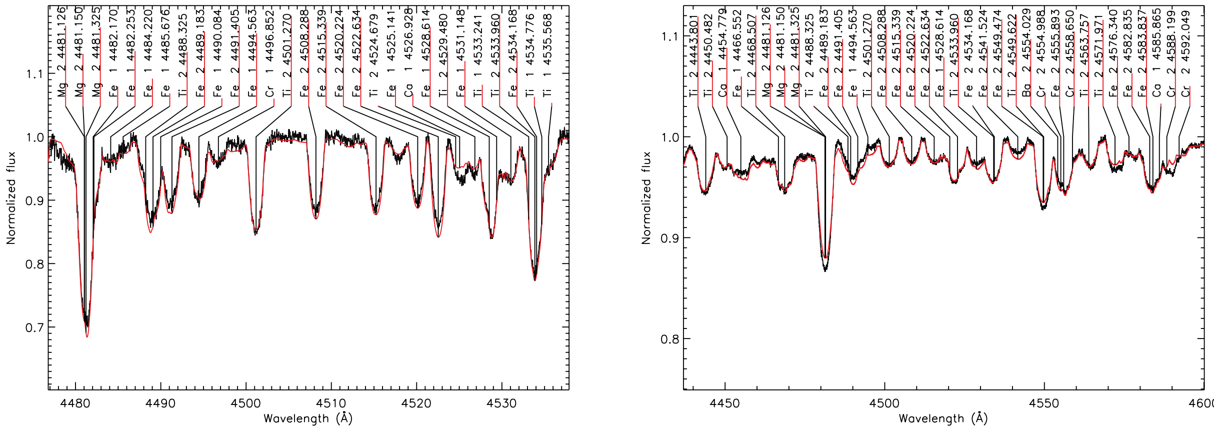

Figure 2. Comparison of our best-fitting model (smooth red) to an observation (noisy black) of HD 142666 (left-hand panel) with a best-fitting $v \sin i$ of 67 km s^{-1}, and HD 9672 (right-hand panel) with a best-fitting $v \sin i$ of 191 km s^{-1} from this method. Identification of the ions with the strongest contribution to the line are indicated above.

this way were used to check those obtained for the same stars from visual comparison and to refine the visual matching process.

We note that the effective temperatures derived from the visual comparison method depend on the assumed (solar) abundance and fixed $\log g = 4.0$. To check the sensitivity of our atmospheric parameter determinations to these assumptions, we compare our $T_{\rm eff}$ values with the results of Folsom et al. (2012), who derive $T_{\rm eff}$ and $\log g$ from detailed spectrum synthesis of a sample of approximately 20 HAeBe stars, simultaneously determining the abundance table and microturbulence parameter. As is illustrated in Fig. 3, the results of our more approximate procedures are in reasonable agreement with those from detailed fitting. Ultimately, the results of the LSD procedure, which are used in particular to determine $v \sin i$, to identify CS and interstellar line features and to diagnose the magnetic field, are only weakly sensitive to the details of the line mask, and errors in the adopted parameters of up to about ±10 to 20 per cent have little impact on the results.

The adopted effective temperatures and surface gravities are summarized in Table 2. The stars whose effective temperature and surface gravity have been determined using a visual inspection or the automatic procedure are labelled with a dagger (†) or a double dagger (‡), respectively. In these two cases no uncertainties have been determined in $\log g$, and the indicated values are estimated at the model grid precision, i.e. ±0.5 dex.

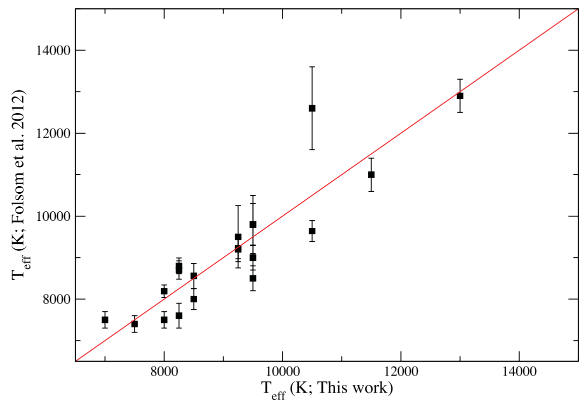

Figure 3. Comparison of effective temperature $T_{\rm eff}$ derived by Folsom et al. (2012) for a sample of ∼20 HAeBe stars, and those derived in this study. The full line indicates a perfect agreement.

4.2 Metallicities

In this work we have assumed a solar metallicity for all our objects (except one, HD 34282, that shows a very low metallicity; Merín et al. 2004) for the following reasons. The spectra of most of the stars of our sample are heavily contaminated with CS emission and/or absorption, making difficult a reliable abundance analysis, and therefore a metallicity determination. However, Folsom et al. (2012), using our data, have isolated the 20 stars of our sample showing only faint CS contamination, and have determined their abundances. They find that about half of them display λ Boo peculiarities, one of them is a magnetic Bp star (V380 Ori A), and all others are chemically normal with solar abundances. We know that magnetic Bp stars have peculiar abundances due to gravitational settling in their atmosphere (Michaud, Charland & Megessier 1981). These peculiarities do not reflect the global chemical composition of the star. The λ Boo peculiarities are not yet fully understood, but are also very likely due to a surface effect (e.g. Folsom et al. 2012). Among these 20 stars, there is therefore no evidence at all that their compositions deviate significantly from that of the Sun. While the Folsom et al. sample concerns only about 30 per cent of our sample, by extrapolation it is reasonable to assume that a large fraction of our targets have a metallicity similar to solar. Acke & Waelkens (2004) have analysed the spectra of 24 HAeBe and Vega-type stars and have found solar metallicities in 21 of them and λ Boo patterns in one of them. Following these works, it is therefore reasonable to assume a solar metallicity in all the stars of our sample (except HD 34282).

4.3 Luminosity determination

The photometric data employed to determine luminosities were taken from the *Hipparcos* and Tycho catalogues (Perryman & ESA 1997), when available, and from Herbst & Shevchenko (1999) and Vieira et al. (2003) otherwise. When a strong photometric variability ($\Delta V > 0.6$ mag) has been observed by *Hipparcos*, we assumed that the reduced brightness of the star was due to variable occultation by CS matter situated around the star. In these few cases, we adopted the brightest *Hipparcos* magnitude $H_{\rm P}$ value as the intrinsic (unocculted) magnitude of the star and we converted it to the Johnson system using the $(v - I)$ colour of *Hipparcos*,

Table 2. Photometric and fundamental parameters. Columns 1 and 2 give the stars' designations. Columns 3–6 give the effective temperature, the surface gravity and their origin. The Johnson V magnitude and $(B-V)$ colour and the reference are indicated in columns 7–9. The visual extinction and magnitude corrected from extinction are given in columns 10 and 11. The distance and its reference are given in columns 12 and 13. The luminosity is given in column 14. Columns 11–13 give the mass, radius and age, while the PMS duration and the predicted radius on the ZAMS are indicated in columns 14 and 15. The measured $v\sin i$ and $v_{\rm rad}$ are given in columns 16 and 17. In columns 14–21, a reference is given when it was not determined in this work. An asterisk (*) indicates a note at the end of the table. All references are indicated at the end of the table.

HD or BD number (1)	Other name (2)	$T_{\rm eff}$ (K) (3)	Ref. (4)	log g (CGS) (5)	Ref. (6)	V (mag) (7)	$(B-V)$ (mag) (8)	Ref. (9)	$A_{\rm V}$ (mag) (10)	V_0 (mag) (11)	d (pc) (12)	Ref. (13)
BD−06 1259	BF Ori	8750 ± 250	ar	4.0 ± 0.5	ar	7.85	−0.028	j	−0.57	8.42	375^{+30}_{-30}	d
BD−06 1253 A	V380 Ori A	10500 ± 500	b	4.0		10.34	0.689	j	3.74	6.59	400^{+40}_{-40}	b
BD−05 1329	T Ori	8500 ± 300	ao	4.2 ± 0.3	ao	10.63	0.53	r	2.64	7.99	375^{+30}_{-30}	d
BD−05 1324	NV Ori	6350 ± 250	ay	4.0		9.90	0.46	r	0.45	9.45	375^{+30}_{-30}	d
BD+41 3731		17000 ± 1000	†	4.0		9.90	0.052	j	1.06	8.84	980^{+500}_{-200}	ai
BD+46 3471	V1578 Cyg	9500 ± 1000	aq	4.0		10.14	0.436	j	2.25	7.89	950^{+80}_{-80}	p
BD+61 154	V594 Cas	13000 ± 500	†	4.0		10.51	0.566	j	3.29	7.22	202^{+97}_{-49}	al
BD+65 1637	V361 Cep	18000 ± 1000	†	4.0		10.83	0.429	j	2.94	7.89	1250^{+50}_{-50}	ah
BD+72 1031	SV Cep	9500 ± 2000	aq	4.0		10.48	0.344	ag	1.87	8.61	400^{+100}_{-100}	v
HD 9672	49 Cet	8900 ± 200	‡	4.5	‡	5.62	0.066	j	0.05	5.57	$59^{+1.0}_{-1.0}$	al
HD 17081	π Cet	12800 ± 200	as	3.77 ± 0.15	as	4.24	−0.122	j	−0.06	4.30	120^{+3}_{-3}	al
HD 31293	AB Aur	9800 ± 700	ao	3.9 ± 0.3	ao	7.03	0.132	j	0.65	6.38	139^{+21}_{-16}	al
HD 31648	MWC 480	8200 ± 300	‡	4.0	‡	7.73	0.160	j	0.10	7.63	137^{+31}_{-21}	al
HD 34282		8625 ± 200	x	4.2 ± 0.20	x	9.92	0.299	j	1.00	8.93	191^{+89}_{-46}	al
HD 35187 B		8900 ± 200	‡	4.0	‡	8.169	0.218	j	0.81	7.36	114^{+41}_{-24}	al
HD 35929		6800 ± 100	at	3.3 ± 0.1	at	8.11	0.438	j	0.69	7.42	375^{+30}_{-30}	d
HD 36112	MWC 758	7800 ± 150	‡	4.0	‡	8.27	0.317	j	0.69	7.59	279^{+94}_{-56}	al
HD 36910	CQ Tau	6750 ± 300	aq	4.0		8.77	0.94	j	2.85	5.92	113^{+29}_{-19}	al
HD 36917	V372 Ori	10000 ± 500	†	4.0		8.03	0.17	an	1.00	7.03	375^{+30}_{-30}	d
HD 36982	LP Ori	20000 ± 1000	†	4.0		8.46	0.09	an	1.55	6.91	375^{+30}_{-30}	d
HD 37258	V586 Ori	9500 ± 500	†	4.0		9.64	0.140	g	0.41	9.23	375^{+30}_{-30}	d
HD 37357		9250 ± 500	am	4.0		8.88	0.13	am	0.37	8.52	375^{+30}_{-30}	d
HD 37806	MWC 120	11000 ± 500	†	4.0		7.91	0.025	j	0.58	7.32	375^{+30}_{-30}	d
HD 38120		11000 ± 500	†	4.0		9.07	0.044	j	0.21	8.86	375^{+30}_{-30}	d
HD 38238	V351 Ori	7750 ± 250	†	4.0		8.89	0.381	j	0.65	8.23	375^{+30}_{-30}	d
HD 50083	V742 Mon	20000 ± 1000	m	3.43 ± 0.15	m	6.91	0.008	j	1.09	5.82	1000^{+100}_{-100}	
HD 52721		22500 ± 2000	m	3.99 ± 0.20	m	6.54	0.016	j	1.28	5.26	670^{140}_{-110}	
HD 53367		29000 ± 2000	†	4.0		6.97	0.357	j	3.29	3.68	255^{+86}_{-51}	al
HD 68695		9000 ± 300	ao	4.3 ± 0.3	ao	9.82	0.10	am	0.49	9.33	570^{+100}_{-100}	i
HD 72106 A		11000 ± 1000	l	4.0 ± 0.5	l	9.00	−0.090	k	−0.09	9.10	289^{+204}_{-85}	j
HD 72106 B		8750 ± 500	l	4.0 ± 0.5	l	9.62	0.20	k	0.10	9.52	289^{+204}_{-85}	j
HD 76534 A		18000 ± 2000	†	4.0		8.35	0.107	j	1.43	6.91	870^{+80}_{-80}	q
HD 98922		10500 ± 500	am	4.0		6.77	0.037	j	0.54	6.24	1150^{+930}_{-360}	al
HD 114981	V958 Cen	17000 ± 2000	†	4.0		7.16	−0.098	j	0.51	6.65	550^{+260}_{-130}	al
HD 135344		6750 ± 250	†	4.0		8.70	0.60	ae	0.96	7.74	142^{+27}_{-27}	aa
HD 139614		7600 ± 300	ao	3.9 ± 0.3	ao	8.40	0.24	am	0.50	7.90	142^{+27}_{-27}	aa
HD 141569		9800 ± 500	ao	4.2 ± 0.4	ao	7.11	0.095	j	0.46	6.65	116^{+9}_{-8}	al
HD 142666	V1026 Sco	7900 ± 200	‡	4.0	‡	8.67	0.50	am	1.60	7.07	145^{+20}_{-20}	af
HD 144432		7500 ± 300	‡	3.5	‡	8.19	0.397	j	0.74	7.45	145^{+20}_{-20}	af
HD 144668	HR 5999	8200 ± 200	‡	3.5	‡	7.00	0.190	j	0.25	6.75	142^{+27}_{-27}	aa
HD 145718	V718 Sco	8100 ± 200	‡	4.0	‡	8.83	0.456	j	1.38	7.45	145^{+20}_{-20}	af
HD 150193	V2307 Oph	9500 ± 500	†	4.0		8.79	0.522	j	2.47	6.32	145^{+20}_{-20}	af

Table 2 – *continued*

ID	$\log(L/\mathrm{L}_\odot)$	$M/\mathrm{M}_\odot$	$R/\mathrm{R}_\odot$	Age (Myr)	t_{PMS} (Myr)	R_{ZAMS} $\mathrm{R}_\odot$	$v \sin i$ (km s^{-1})	v_{rad} (km s^{-1})
(1) or (2)	(14)	(15)	(16)	(17)	(18)	(19)	(20)	(21)
BD−06 1259	$1.75^{+0.7}_{-0.7}$	$2.58^{+0.14}_{-0.14}$	$3.26^{+0.31}_{-0.31}$	$3.15^{+0.58}_{-0.44}$	$5.1^{+1.0}_{-0.8}$	$1.88^{+0.06}_{-0.06}$	39 ± 9	22 ± 6
BD−06 1253 A	$1.99^{+0.22b}_{-0.22}$	$2.87^{+0.52b}_{-0.32}$	$3.00^{+1.1b}_{-0.8}$	$2.5^{+1.0}_{-1.0}$	$3.56^{+1.3}_{-1.5}$	$1.99^{+0.10}_{-0.10}$	6.7 ± 1.1^{b}	$[27.3,28.2]^{b}$
BD−05 1329	$1.97^{+0.07}_{-0.07}$	$3.13^{+0.19}_{-0.19}$	$4.47^{+0.46}_{-0.46}$	$1.77^{+0.38}_{-0.32}$	$2.66^{+0.60}_{-0.49}$	$2.10^{+0.07}_{-0.07}$	147 ± 9	29 ± 8
BD−05 1324	$1.32^{+0.07}_{-0.07}$	$2.28^{+0.18}_{-0.16}$	$3.77^{+0.41}_{-0.41}$	$3.7^{+1.0}_{-0.9}$	$7.6^{+2.0}_{-1.7}$	$1.75^{+0.07}_{-0.07}$	74 ± 7	30 ± 5
BD+41 3731	$3.03^{+0.36}_{-0.20}$	$5.50^{+1.37}_{-0.38}$	$3.8^{+0.8}_{-0.8}$	$0.24^{+0.18}_{-0.15}$	$0.344^{+0.042}_{-0.119}$	$2.89^{+0.11}_{-0.11}$	345 ± 27	-14 ± 22
BD+46 3471	$2.84^{+0.07}_{-0.08}$	$5.9^{+0.6}_{-0.5}$	$9.7^{+1.9}_{-1.9}$	$0.06^{+0.06}_{-0.06}$	$0.31^{+0.05}_{-0.06}$	$3.00^{+0.15}_{-0.15}$	199 ± 11	-3 ± 9
BD+61 154	1.95^{+34}_{-24}	$3.41^{+0.38}_{-0.38}$	$2.42^{+0.35}_{-0.35}$	$2.2^{+0.9}_{-0.9}$	$2.2^{+0.9}_{-0.9}$	$2.20^{+0.14}_{-0.14}$	112 ± 24	-16 ± 18
BD+65 1637	$3.620^{+0.034}_{-0.035}$	$8.11^{+0.24}_{-0.23}$	$6.7^{+0.7}_{-0.7}$	$0.035^{+0.012}_{-0.010}$	$0.153^{+0.012}_{-0.010}$	$3.56^{+0.05}_{-0.05}$	278 ± 27	-26 ± 20
BD+72 1031	$1.82^{+0.19}_{-0.25}$	$2.62^{+0.59}_{-0.34}$	$3.0^{+1.1}_{-1.1}$	$3.2^{+1.9}_{-1.6}$	$4.8^{+2.8}_{-2.4}$	$1.89^{+0.14}_{-0.14}$	180 ± 15	-9 ± 11
HD 9672	$1.297^{+0.015}_{-0.014}$	$2.13^{+0.08}_{-0.07}$	$1.88^{+0.09}_{-0.09}$	$7.0^{+1.1}_{-1.3}$	$9.0^{+1.0}_{-1.0}$	$1.690^{+0.030}_{-0.030}$	195 ± 6	13.1 ± 4.6
HD 17081	$2.750^{+0.022}_{-0.022}$	$4.65^{+0.08}_{-0.08}$	$4.84^{+0.19}_{-0.19}$	$0.279^{+0.012}_{-0.023}$	$0.469^{+0.012}_{-0.021}$	$2.630^{+0.030}_{-0.030}$	19.9 ± 0.9	[11.0,12.7]
HD 31293	$1.76^{+0.12}_{-0.11}$	$2.50^{+0.29}_{-0.13}$	$2.62^{+0.44}_{-0.44}$	$3.7^{+0.6}_{-0.8}$	$5.6^{+1.1}_{-1.7}$	$1.84^{+0.06}_{-0.06}$	116 ± 6	24.7 ± 4.7
HD 31648	$1.18^{+0.18}_{-0.15}$	$1.93^{+0.09}_{-0.14}$	$1.93^{+0.32}_{-0.32}$	$7.8^{+4.5}_{-1.5}$	$12.9^{+3.3}_{-1.8}$	$1.60^{+0.06}_{-0.06}$	97.5 ± 4.7	12.9 ± 3.5
HD 34282	$1.13^{+0.27x}_{-0.22}$	$1.59^{+0.30x}_{-0.07}$	$1.66^{+0.62x}_{-0.37}$	$6.4^{+2.6x}_{-1.9}$			105 ± 6	16.2 ± 4.8
HD 35187 B	$1.15^{+0.27}_{-0.20}$	$1.93^{+0.28}_{-0.04}$	$1.58^{+0.02}_{-0.02}$	$10.7^{+3.7}_{-5.2}$	$12.9^{+1.4}_{-4.5}$	$1.60^{+0.04}_{-0.04}$	93.3 ± 2.8	27.0 ± 2.1
HD 35929	$2.12^{+0.07}_{-0.07}$	$4.13^{+0.23}_{-0.24}$	$8.1^{+0.7}_{-0.7}$	$0.16^{+0.49}_{-0.08}$	$0.68^{+0.54}_{-0.13}$	$2.46^{+0.08}_{-0.08}$	61.8 ± 2.2	21.1 ± 1.8
HD 36112	$1.81^{+0.25}_{-0.19}$	$2.90^{+0.67}_{-0.43}$	$4.4^{+0.9}_{-0.9}$	$2.1^{+1.1}_{-1.1}$	$3.4^{+2.4}_{-1.8}$	$2.01^{+0.17}_{-0.17}$	54.1 ± 4.9	17.8 ± 3.7
HD 36910	$1.69^{+0.20}_{-0.16}$	$2.93^{+0.54}_{-0.37}$	$5.1^{+0.9}_{-0.9}$	$1.9^{+0.9}_{-0.8}$	$3.3^{+1.9}_{-1.5}$	$2.02^{+0.15}_{-0.15}$	98 ± 5	35.7 ± 4.5
HD 36917	$2.39^{+0.07}_{-0.07}$	$3.98^{+0.25}_{-0.24}$	$5.2^{+0.6}_{-0.6}$	$0.72^{+0.29}_{-0.42}$	$1.06^{+0.33}_{-0.45}$	$2.41^{+0.09}_{-0.09}$	127.1 ± 4.6	26.3 ± 3.6
HD 36982	$3.22^{+0.07}_{-0.07}$	$6.70^{+0.64}_{-0.37}$	$3.42^{+0.30}_{-0.30}$	$0.20^{+0.07}_{-0.07}$	$0.230^{+0.043}_{-0.030}$	$3.22^{+0.10}_{-0.10}$	88 ± 8	30 ± 6
HD 37258	$1.44^{+0.07}_{-0.07}$	$2.28^{+0.15}_{-0.16}$	$1.94^{+0.24}_{-0.24}$	$5.9^{+1.8}_{-1.5}$	$7.5^{+1.9}_{-1.4}$	$1.75^{+0.07}_{-0.07}$	200 ± 14	31 ± 12
HD 37357	$1.72^{+0.07}_{-0.07}$	$2.47^{+0.13}_{-0.11}$	$2.83^{+0.35}_{-0.35}$	$3.7^{+0.6}_{-0.5}$	$5.8^{+1.0}_{-0.9}$	$1.83^{+0.05}_{-0.05}$	124 ± 7	21.4 ± 4.7
HD 37806	$2.45^{+0.07}_{-0.07}$	$3.94^{+0.23}_{-0.23}$	$4.6^{+0.5}_{-0.5}$	$0.88^{+0.21}_{-0.51}$	$1.18^{+0.25}_{-0.53}$	$2.39^{+0.08}_{-0.08}$	120 ± 27	47 ± 21
HD 38120	$1.62^{+0.07}_{-0.07}$	$2.49^{+0.09}_{-0.09}$	$1.91^{+0.11}_{-0.11}$	$5.1^{+0.5}_{-0.5}$	$5.6^{+0.8}_{-0.8}$	$1.840^{+0.040}_{-0.040}$	97 ± 17	28 ± 12
HD 38238	$1.79^{+0.07}_{-0.07}$	$2.88^{+0.18}_{-0.18}$	$4.38^{+0.44}_{-0.44}$	$2.16^{+0.46}_{-0.38}$	$3.5^{+0.8}_{-0.6}$	$2.00^{+0.07}_{-0.07}$	99.8 ± 4.2	15.0 ± 2.9
HD 50083	$4.15^{+0.12}_{-0.12}$	$12.1^{+1.1}_{-1.1}$	$10.0^{+1.0}_{-1.0}$	$0.004^{+0.006}_{-0.006}$	$0.033^{+0.035}_{-0.035}$	$7.6^{+3.4}_{-3.4}$	233 ± 22	-0.4 ± 1.2
HD 52721	$3.77^{+0.35}_{-0.31}$	$9.1^{+2.4}_{-1.4}$	$5.0^{+1.2}_{-1.2}$	$0.044^{+0.073}_{-0.030}$	$0.12^{+0.06}_{-0.06}$	$3.78^{+0.33}_{-0.33}$	215 ± 18	21 ± 14
HD 53367	$4.50^{+0.25}_{-0.20}$	$16.1^{+2.7}_{-1.6}$	$7.1^{+1.6}_{-1.6}$	$0.008^{+0.016}_{-0.008}$	$0.036^{+0.000}_{-0.035}$	$5.13^{+0.29}_{-0.29}$	41 ± 7	47.2 ± 4.8
HD 68695	$1.80^{+0.14}_{-0.17}$	$2.64^{+0.31}_{-0.30}$	$3.3^{+0.6}_{-0.6}$	$3.0^{+1.2}_{-0.8}$	$4.7^{+2.3}_{-1.4}$	$1.90^{+0.13}_{-0.13}$	43.8 ± 2.6	20.3 ± 1.7
HD 72106 A	$1.34^{+0.28l}_{-0.26}$	$2.40^{+0.3l}_{-0.3}$	$1.3^{+0.5l}_{-0.5}$	9.0^{+4}_{-3}	9.0^{+4}_{-3}	$1.3^{+0.5}_{-0.5}$	41.0 ± 0.3^{l}	22 ± 1^{l}
HD 72106 B	$0.96^{+0.27l}_{-0.27}$	$1.9^{+0.2l}_{-0.2}$	$1.3^{+0.5l}_{-0.5}$	9.0^{+4}_{-3}	9.0^{+4}_{-3}	$1.3^{+0.5}_{-0.5}$	53.9 ± 1.0^{l}	22 ± 1^{l}
HD 76534 A	$3.75^{+0.08}_{-0.08}$	$9.0^{+0.6}_{-0.6}$	$7.7^{+1.6}_{-1.6}$	$0.021^{+0.018}_{-0.013}$	$0.122^{+0.019}_{-0.022}$	$3.76^{+0.13}_{-0.13}$	68 ± 30	23 ± 18
HD 98922	$3.77^{+0.52}_{-0.32}$						50.0 ± 3.0	0.2 ± 2.2
HD 114981	$3.56^{+0.34}_{-0.24}$	$7.9^{+2.4}_{-1.3}$	$7.0^{+2.0}_{-2.0}$	$0.038^{+0.064}_{-0.038}$	$0.16^{+0.08}_{-0.08}$	$3.51^{+0.33}_{-0.33}$	239 ± 13	-50 ± 11
HD 135344	$1.16^{+0.15}_{-0.18}$	$1.90^{+0.25}_{-0.24}$	$2.8^{+0.6}_{-0.6}$	$6.6^{+3.4}_{-2.0}$	$13.6^{+6.9}_{-4.4}$	$1.58^{+0.11}_{-0.11}$	82.4 ± 2.0	-0.0011 ± 0.0006
HD 139614	$1.10^{+0.15}_{-0.18}$	$1.76^{+0.15}_{-0.08}$	$2.06^{+0.42}_{-0.42}$	$8.8^{+4.5}_{-1.9}$	$17.2^{+2.7}_{-3.9}$	$1.520^{+0.040}_{-0.040}$	24.1 ± 3.0	0.3 ± 2.3
HD 141569	$1.49^{+0.06}_{-0.06}$	$2.33^{+0.20}_{-0.12}$	$1.94^{+0.21}_{-0.21}$	$5.7^{+1.3}_{-1.4}$	$7.1^{+1.4}_{-1.7}$	$1.77^{+0.05}_{-0.05}$	228 ± 10	-12 ± 7
HD 142666	$1.44^{+0.11}_{-0.13}$	$2.15^{+0.20}_{-0.19}$	$2.82^{+0.41}_{-0.41}$	$5.0^{+1.6}_{-1.1}$	$9.2^{+3.1}_{-2.2}$	$1.70^{+0.08}_{-0.08}$	65.3 ± 3.1	-7.0 ± 2.7
HD 144432	$1.28^{+0.11}_{-0.13}$	$1.95^{+0.18}_{-0.16}$	$2.59^{+0.40}_{-0.40}$	$6.4^{+1.8}_{-1.4}$	$12.4^{+3.7}_{-3.0}$	$1.61^{+0.07}_{-0.07}$	78.8 ± 4.2	-3.0 ± 3.5
HD 144668	$1.56^{+0.15}_{-0.18}$	$2.31^{+0.29}_{-0.28}$	$3.0^{+0.6}_{-0.6}$	$4.2^{+2.0}_{-1.2}$	$7.2^{+3.7}_{-2.3}$	$1.77^{+0.12}_{-0.12}$	199 ± 11	-10 ± 8
HD 145718	$1.29^{+0.11}_{-0.13}$	$1.93^{+0.14}_{-0.08}$	$2.25^{+0.33}_{-0.33}$	$7.4^{+0.7}_{-1.7}$	$12.8^{+1.8}_{-2.5}$	$1.60^{+0.04}_{-0.04}$	113.4 ± 3.4	-3.6 ± 2.3
HD 150193	$1.79^{+0.11}_{-0.13}$	$2.56^{+0.22}_{-0.19}$	$2.89^{+0.48}_{-0.48}$	$3.3^{+0.9}_{-0.7}$	$5.2^{+1.5}_{-1.2}$	$1.87^{+0.08}_{-0.08}$	108 ± 5	-4.9 ± 3.9

and the conversion table of the *Hipparcos* and Tycho catalogues (Perryman & ESA 1997, p. 59). We used the visual magnitude (V) corrected for reddening (A_{v}) obtained from the colour excess $E(B-V)$ and a total-to-selective extinction R_{v} [$A_{\mathrm{v}} = R_{\mathrm{v}} \times E(B-V)$] of 5.0 (Hernández et al. 2004), the bolometric corrections and the distances of the stars, to estimate their luminosity. The intrinsic $(B-V)$ and bolometric corrections of all stars have been obtained from the effective temperature reported in Table 2 and the calibration of Kenyon & Hartmann (1995). The errors on the luminosities have been determined by propagating the error on the distances. For

Table 2 – *continued*

HD or BD number (1)	Other name (2)	T_{eff} (K) (3)	Ref. (4)	$\log g$ (CGS) (5)	Ref. (6)	V (mag) (7)	$(B-V)$ (mag) (8)	Ref. (9)	A_{V} (mag) (10)	V_0 (mag) (11)	d (pc) (12)	Ref. (13)
HD 152404 A	AK Sco A	6500 ± 100	c	4.0		8.839	0.622	w	1.06	7.78	103^{+27}_{-18}	al
HD 152404 B	AK Sco B	6500 ± 100	c	4.0								
HD 163296		9200 ± 300	ao	4.2 ± 0.3	ao	6.86	0.092	j	0.32	6.54	119^{+12}_{-10}	al
HD 169142		7500 ± 200	ao	4.3 ± 0.2	ao	8.15	0.28	am	−0.30	8.45	145^{+40}_{-40}	ak
HD 174571	MWC 610	21000 ± 1500	m	4.00 ± 0.10	m	8.87	0.610	j	4.15	4.72	540^{+80}_{-70}	
HD 176386		11500 ± 350	‡	4.5	‡	7.22	0.121	j	1.00	6.22	128^{+15}_{-12}	al
HD 179218		9640 ± 250	ao	3.9 ± 0.2	ao	7.40	0.094	j	0.77	6.63	254^{+45}_{-33}	al
HD 190073	V1295 Aql	9250 ± 250	e	3.5 ± 0.5	e	7.84	0.113	j	0.43	7.41		
HD 200775 A	MWC 361 A	18600 ± 2000	a	3.5	a	7.34	0.306	j	2.43	4.91	429^{+156}_{-90}	j
HD 200775 B	MWC 361 B	18600 ± 2000	a	3.6	a							
HD 203024 A		9250	†	4.0		8.80	0.40	aj	1.86	6.94	420^{+50}_{-50}	u
HD 203024 B		6500	†	4.0								
HD 216629 A	IL Cep A	19000	†	4.0		9.34	-0.240	j	-0.25	9.59	720^{+190}_{-150}	f
HD 216629 B	IL Cep B	19000	†	4.0								
HD 244314	V1409 Ori	9250 ± 500	am	4.0		10.19	0.22	z	0.96	9.23	375^{+30}_{-30}	d
HD 244604	V1410 Ori	8200 ± 200	‡	4.0	‡	8.99	0.255	g	0.57	8.41	375^{+30}_{-30}	d
HD 245185	V1271 Ori	9500 ± 750	ao	4.0 ± 0.4	ao	9.96	0.070	s	0.21	9.75	450^{+50}_{-50}	ab
HD 249879		9000 ± 1000	†	4.0		10.64	0.05	am	−0.04	10.68	2000^{+500}_{-500}	am
HD 250550	V1307 Ori	12000 ± 1500	†	4.0		9.51	0.044	j	0.68	8.83		
HD 259431	V700 Mon	14000 ± 1000	†	4.0		8.71	0.274	j	2.02	6.69	660^{+100}_{-100}	t
HD 275877	XY Per	9000 ± 500	ay	4.0		9.04	0.47	ad	1.75	7.29	120^{+87}_{-35}	j
HD 278937	IP Per	8500 ± 250	ao	4.1 ± 0.2	ao	10.36	0.31	y	0.95	9.41	320^{+30}_{-30}	h
HD 287823 A		10000	†	4.0		9.71	0.223	j	1.26	8.45	375^{+30}_{-30}	d
HD 287823 B		7000	†	4.0								
HD 287841	V346 Ori	7550 ± 250	av	3.5 ± 0.4	av	10.21	0.199	j	0.09	10.11	375^{+30}_{-30}	d
HD 290409 A		9000 ± 500	†	4.0		10.02	0.09	am	0.17	9.85	375^{+30}_{-30}	o
HD 290500		9000 ± 500	†	4.0		11.04	0.31	n	1.26	9.77	375^{+30}_{-30}	d
HD 290770		11000 ± 1000	†	4.0		9.27	0.03	am	0.61	8.66	375^{+30}_{-30}	d
HD 293782	UX Ori	9250 ± 500	ax	4.0	ax	8.53	0.615	j	3.06	5.47	375^{+30}_{-30}	d
HD 344361	WW Vul	9000 ± 1000	ar	4.0		10.74	0.41	r	2.04	8.70	700^{+260}_{-150}	ap
	LkHa 215 A	14000	†	4.0		10.54	0.52	r	3.25	7.29	900^{+100}_{-100}	ac
	LkHa 215 B	14000	†	4.0								
	MWC 1080	30000	aw	4.0		11.58	1.197	j	7.09	4.49	2300^{+600}_{-600}	
	VV Ser	14000 ± 2000	aq	4.0		11.92	0.96	r	5.35	6.57	260^{+100}_{-100}	az
	VX Cas	9500 ± 1500	aq	4.0		11.28	0.32	r	1.67	9.61	620^{+60}_{-60}	ap

the double-lined spectroscopic binaries (SB2) we have attempted a visual estimation of their luminosity ratio using the observed ratio of the individual spectral line depths of our data. However, in all but one of the systems we also had to adjust the temperatures of both components at the same time. The results being highly inaccurate we have not attempted an estimation of their error bars and therefore no errors on the luminosity of the individual components are reported for these systems. In the case of AK Sco, well-constrained temperatures of both components had been obtained by Alencar et al. (2003). It was therefore possible to derive an error bar on the luminosity ratio of the system, and therefore on the individual luminosities (see Appendix A and Table 2).

All the quantities are summarized in Table 2, while the sources of the data are detailed, star by star, in Appendix A. For three stars (HD 50083, HD 52721, HD 174571) no reliable distance could be found in the literature. We have therefore estimated their luminosity from their effective temperature and surface gravity by comparing their position in a $\log g$–T_{eff} diagram with theoretical evolutionary tracks (described in Section 4.4).

4.4 Mass and radius determination

We placed all the stars in an HR diagram (Fig. 4), with the error bars when available, and compared their positions with evolutionary tracks calculated with the CESAM stellar evolutionary code (Morel 1997) version 2K. Using a 2D linear interpolation and a grid of 120 evolutionary tracks with masses from 1 to 20 $\mathrm{M}_{\odot}$, and mass steps

Table 2 – *continued*

ID	$\log(L/\mathrm{L}_{\odot})$	$M/\mathrm{M}_{\odot}$	$R/\mathrm{R}_{\odot}$	Age (Myr)	t_{PMS} (Myr)	R_{ZAMS} $R_{\odot}$	$v \sin i$ (km s^{-1})	v_{rad} (km s^{-1})
(1) or (2)	(14)	(15)	(16)	(17)	(18)	(19)	(20)	(21)
HD 152404 A	$0.95^{+0.21}_{-0.21}$	$1.66^{+0.29}_{-0.21}$	$2.4^{+0.5}_{-0.5}$	$9.3^{+3.8}_{-3.3}$	20^{+10}_{-8}	$1.48^{+0.10}_{-0.10}$	18.2 ± 1.7	-17.0 ± 1.3
HD 152404 B	$0.71^{+0.21}_{-0.21}$	$1.43^{+0.20}_{-0.09}$	$1.79^{+0.38}_{-0.38}$	$13.7^{+3.6}_{-4.3}$	31^{+6}_{-10}	$1.37^{+0.04}_{-0.04}$	17.6 ± 0.9	14.3 ± 0.9
HD 163296	$1.52^{+0.08}_{-0.08}$	$2.23^{+0.22}_{-0.07}$	$2.28^{+0.23}_{-0.23}$	$5.10^{+0.31}_{-0.77}$	$8.1^{+0.9}_{-2.1}$	$1.73^{+0.03}_{-0.03}$	129 ± 8	-9 ± 6
HD 169142	$0.88^{+0.21}_{-0.28}$	$1.69^{+0.06}_{-0.14}$	$1.64^{+0.20}_{-0.20}$	$13.5^{+11.2}_{-4.7}$	$19.2^{+5.5}_{-1.9}$	$1.49^{+0.06}_{-0.06}$	47.8 ± 2.3	-0.4 ± 2.0
HD 174571	$3.58^{+0.21}_{-0.21}$	$8.0^{+1.2}_{-1.0}$	$4.7^{+0.6}_{-0.6}$	$0.065^{+0.050}_{-0.026}$	$0.161^{+0.060}_{-0.043}$	$3.53^{+0.24}_{-0.24}$	219 ± 31	14 ± 24
HD 176386	$1.91^{+0.09}_{-0.09}$	$3.02^{+0.23}_{-0.26}$	$2.28^{+0.24}_{-0.24}$	$2.8^{+1.0}_{-0.8}$	$3.0^{+1.1}_{-0.7}$	$2.05^{+0.10}_{-0.10}$	175 ± 6	-2 ± 5
HD 179218	$2.26^{+0.14}_{-0.12}$	$3.66^{+0.44}_{-0.34}$	$4.8^{+0.7}_{-0.7}$	$1.08^{+0.48}_{-0.70}$	$1.5^{+0.6}_{-0.8}$	$2.29^{+0.12}_{-0.12}$	68.8 ± 2.9	15.1 ± 2.3
HD 190073	$1.92^{+0.12\,e}_{-0.12}$	$2.85^{+0.25\,e}_{-0.25}$	$3.60^{+0.5\,e}_{-0.5}$	$2.40^{+0.7}_{-0.6}$	$3.6^{+1.3}_{-1.0}$	$1.99^{+0.10}_{-0.10}$	[0-8.3][d]	0.21 ± 0.10[d]
HD 200775 A	$3.95^{+0.30\,a}_{-0.30}$	$10.7^{+2.5\,a}_{-2.5}$	$10.4^{+4.9\,a}_{-4.9}$	$0.016^{+0.009}_{-0.009}$	$0.07^{+0.07}_{-0.07}$	$4.1^{+0.5}_{-0.5}$	26 ± 2[a]	[−23.3,8.2][a]
HD 200775 B	$3.77^{+0.30\,a}_{-0.30}$	$9.3^{+2.1\,a}_{-2.1}$	$8.3^{+3.9\,a}_{-3.9}$	$0.016^{+0.009}_{-0.009}$	$0.12^{+0.08}_{-0.06}$	$3.8^{+0.4}_{-0.4}$	59 ± 5[a]	[−21.1,9.3][a]
HD 203024 A	1.88	2.8	3.4	2.7	4.0	1.9	162 ± 11	-14 ± 9
HD 203024 B	0.93	1.6	2.3	9.3	21.1	1.5	57.1 ± 3.8	[−10.5,−5.3]
HD 216629 A	$2.58^{+0.20}_{-0.20}$						179 ± 27	[−39,31]
HD 216629 B							152 ± 33	[−87,−30]
HD 244314	$1.45^{+0.07}_{-0.07}$	$2.33^{+0.08}_{-0.23}$	$2.07^{+0.26}_{-0.26}$	$4.78^{+2.40}_{-0.19}$	$7.1^{+2.8}_{-0.7}$	$1.77^{+0.10}_{-0.10}$	51.9 ± 2.2	22.5 ± 1.8
HD 244604	$1.74^{+0.07}_{-0.07}$	$2.66^{+0.15}_{-0.15}$	$3.69^{+0.34}_{-0.34}$	$2.79^{+0.52}_{-0.41}$	$4.6^{+1.0}_{-0.8}$	$1.91^{+0.06}_{-0.06}$	98.3 ± 1.8	26.8 ± 1.6
HD 245185	$1.40^{+0.09}_{-0.10}$	$2.19^{+0.27}_{-0.12}$	$1.85^{+0.20}_{-0.20}$	$6.9^{+2.0}_{-2.5}$	$8.7^{+1.8}_{-2.7}$	$1.71^{+0.06}_{-0.06}$	118 ± 22	16 ± 16
HD 249879	$2.31^{+0.19}_{-0.25}$	$4.0^{+0.8}_{-0.8}$	$5.9^{+1.8}_{-1.8}$	$0.7^{+1.0}_{-0.5}$	$1.1^{+1.3}_{-0.6}$	$2.40^{+0.27}_{-0.27}$	254 ± 26	11 ± 20
HD 250550							79 ± 9	-22 ± 8
HD 259431	$3.35^{+0.12}_{-0.14}$	$7.1^{+0.8}_{-0.8}$	$8.0^{+1.6}_{-1.6}$	$0.059^{+0.035}_{-0.041}$	$0.218^{+0.040}_{-0.053}$	$3.32^{+0.20}_{-0.20}$	83 ± 11	26 ± 8
HD 275877	$1.21^{+0.47}_{-0.30}$	$1.95^{+0.46}_{-0.09}$	$1.65^{+0.11}_{-0.11}$	10^{+6}_{-6}	$12.4^{+3.1}_{-6.2}$	$1.61^{+0.06}_{-0.06}$	224 ± 12	2 ± 10
HD 278937	$1.21^{+0.08}_{-0.09}$	$1.86^{+0.10}_{-0.06}$	$2.10^{+0.23}_{-0.23}$	$8.19^{+0.40}_{-1.18}$	$14.3^{+1.4}_{-2.2}$	$1.570^{+0.030}_{-0.030}$	79.8 ± 2.9	13.7 ± 2.1
HD 287823 A	1.79	2.5	2.6	3.5	5.2	1.9	10.3 ± 1.5	-0.3 ± 1.1
HD 287823 B	0.82	1.6	1.8	11.9	24.2	1.4	8.2 ± 3.3	54.0 ± 1.6
HD 287841	$1.05^{+0.07}_{-0.07}$	$1.72^{+0.15}_{-0.05}$	$1.96^{+0.20}_{-0.20}$	$9.3^{+0.6}_{-0.8}$	$18.2^{+1.6}_{-4.2}$	$1.510^{+0.020}_{-0.020}$	115.8 ± 4.2	20.0 ± 3.6
HD 290409 A	$1.32^{+0.06}_{-0.06}$	$2.04^{+0.18}_{-0.18}$	$1.75^{+0.20}_{-0.20}$	$10.5^{+4.8}_{-4.8}$	$11.8^{+3.5}_{-3.5}$	$1.64^{+0.09}_{-0.09}$	250 ± 120	1 ± 70
HD 290500	$1.22^{+0.07}_{-0.07}$	$1.96^{+0.21}_{-0.06}$	$1.68^{+0.09}_{-0.09}$	$9.8^{+2.9}_{-3.7}$	$12.3^{+1.3}_{-3.4}$	$1.61^{+0.03}_{-0.03}$	85 ± 15	29 ± 11
HD 290770	$1.91^{+0.07}_{-0.07}$	$2.86^{+0.27}_{-0.21}$	$2.49^{+0.44}_{-0.44}$	$2.76^{+0.86}_{-0.33}$	$3.6^{+1.0}_{-0.9}$	$1.99^{+0.08}_{-0.08}$	240 ± 100	4 ± 60
HD 293782	$2.98^{+0.07}_{-0.07}$	$6.72^{+0.42}_{-0.43}$	$12.1^{+1.5}_{-1.5}$	$0.009^{+0.027}_{-0.009}$	$0.229^{+0.034}_{-0.226}$	$3.22^{+0.12}_{-0.12}$	221 ± 13	12 ± 10
HD 344361	$2.23^{+0.27}_{-0.21}$	$3.7^{+1.0}_{-0.6}$	$5.4^{+1.4}_{-1.4}$	$0.9^{+0.9}_{-0.8}$	$1.0^{+1.0}_{-1.0}$	$2.31^{+0.22}_{-0.22}$	196 ± 8	-4 ± 8
LkHa 215 A	$3.08^{+0.10\star}_{-0.10}$	5.8	5.9	0.1	0.3	3.0	210 ± 70	0 ± 40
LkHa 215 B	$3.08^{+0.10\star}_{-0.10}$	5.8	5.9	0.1	0.3	3.0	11.7 ± 4.6	[12,22]
MWC 1080	$5.77^{+0.20}_{-0.26}$	17.4	7.3	0.0028	0.033	5.4		
VV Ser	$2.51^{+0.28}_{-0.42}$	$4.0^{+0.8}_{-0.8}$	$3.1^{+0.9}_{-0.9}$	$0.64^{+1.91}_{-0.35}$	$0.76^{+1.78}_{-0.33}$	$2.43^{+0.29}_{-0.29}$	124 ± 24	51 ± 18
VX Cas	$1.78^{+0.08}_{-0.09}$	$2.55^{+0.37}_{-0.14}$	$2.9^{+0.8}_{-0.8}$	$3.4^{+0.6}_{-1.0}$	$5.3^{+1.0}_{-1.9}$	$1.86^{+0.06}_{-0.06}$	158 ± 23	-9 ± 18

Note. ⋆Assuming that both components have the same temperature, and therefore the same luminosity. References: †Visual temperature determination; ‡Automatic temperature determination; (a) Alecian et al. (2008a); (b) Alecian et al. (2009b); (c) Alencar et al. (2003); (d) Brown, de Geus & de Zeeuw (1994); (e) Catala et al. (2007); (f) Crawford & Barnes (1970); (g) de Winter et al. (2001); (h) de Zeeuw et al. (1999); (i) Eggen (1986); (j) ESA (1997); (k) Fabricius & Makarov (2000); (l) Folsom et al. (2008); (m) Frémat et al. (2006); (n) Guetter (1979); (o) Guetter (1981); (p) Harvey et al. (2008); (q) Herbst (1975); (r) Herbst & Shevchenko (1999); (s) Høg et al. (2000); (t) Kharchenko et al. (2005); (u) Kun, Vinkó & Szabados (2000); (v) Kun (1998); (w) Manset, Bastien & Bertout (2005); (x) Merín et al. (2004); (y) Miroshnichenko et al. (2001); (z) Miroshnichenko et al. (1999a); (aa) Müller et al. (2011); (ab) Murdin & Penston (1977); (ac) Oliver, Masheder & Thaddeus (1996); (ad) Oudmaijer et al. (2001); (ae) Oudmaijer et al. (1992); (af) Preibisch & Mamajek (2008); (ag) Rostopchina et al. (2000); (ah) Shevchenko & Yakubov (1989); (ai) Shevchenko, Ibragimov & Chenysheva (1991); (aj) Simbad (http://simbad.u-strasbg.fr/simbad/); (ak) Sylvester et al. (1996); (al) van Leeuwen (2007); (am) Vieira et al. (2003); (an) Wolff et al. (2004); (ao) Folsom et al. (2012); (ap) Montesinos et al. (2009); (aq) Hernández et al. (2004); (ar) Mora et al. (2004); (as) Fossati et al. (2009); (at) Miroshnichenko et al. (2004); (au) Hernández et al. (2005); (av) Bernabei et al. (2009); (aw) Hillenbrand et al. (1992); (ax) Mora et al. (2002); (ay) Mora et al. (2001); (az) Straižys, Černis & Bartašiūte (1996).

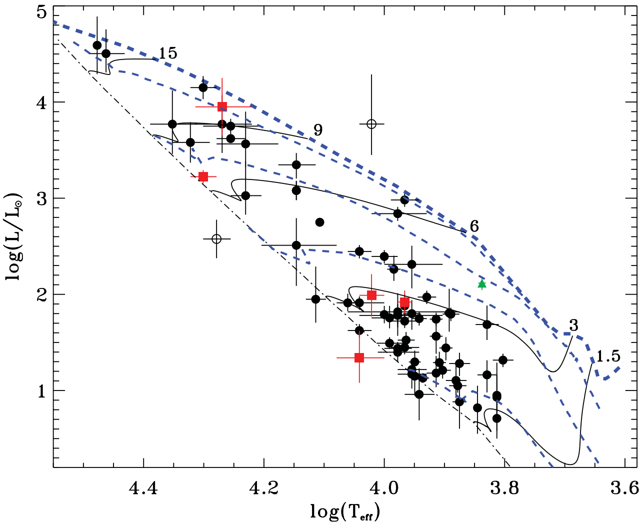

Figure 4. Magnetic (red squares) and non-magnetic (black circle) Herbig Ae/Be stars plotted in an HR diagram. The green triangle is the candidate magnetic star HD 35929. Open circles correspond to HD 98922 (above the birthline) and IL Cep (below the ZAMS) that fall outside of the PMS region of the HR diagram, whose positions cannot be reproduced with the theoretical evolutionary tracks considered in this paper. The CESAM PMS evolutionary tracks for 1.5, 3, 6, 9 and 15 $\mathrm{M_{\odot}}$ (black full lines), 0.01, 0.1, 1 and 10 Myr isochrones (blue thin-dashed lines), and ZAMS (black dot–dashed line) are also plotted. The birthline taken from BM01 is plotted with a blue thick-dashed line.

varying between 0.01 and 1 $\mathrm{M_{\odot}}$ (depending on the mass and the position of the stars in the HR diagram), we determined the mass, radius and age of each star.

The errors have been determined using the intersection of the evolutionary tracks with the error ellipses, as defined by the errors in effective temperature, luminosity or surface gravity. When the ellipses are intersecting the ZAMS or the birthline, only the portion of the ellipse between the birthline and the ZAMS was considered.

The ages have been measured from the birthline, i.e the locus in the HR diagram where the newly formed stars become observable at optical wavelength, meaning that the CS matter in which the stars were buried during the protostellar phase becomes optically thin. We used the birthline of BM01 that has been computed with a mass accretion rate increasing with the luminosity of the growing star. We favoured a birthline calculated with a modulated accretion rate (instead of a constant accretion rate as computed by Palla & Stahler 1993) as it better fits the upper envelope of the distribution of massive Herbig Be stars in the HR diagram (see Fig. 4). Furthermore, Palla & Stahler (1993, hereafter PS93) argue that a constant accretion rate of $10^{-5}\,\mathrm{M_{\odot}\,yr^{-1}}$ during the protostellar phase is a good approximation as it fits well the upper envelope of the known Herbig Ae/Be stars. However, their work was only including HAeBe stars of masses lower than 6 $\mathrm{M_{\odot}}$. Since their work, more massive stars have been identified as Herbig Be (e.g. Vieira et al. 2003; Martayan et al. 2008), while intermediate-mass T Tauri stars that are cooler and younger than Herbig Ae/Be star and that are identified as the progenitors of the Herbig Ae/Be phases, have also been found (e.g. Wolff et al. 2004; Hussain et al. 2009). The latter are filling the right-hand part of the HR diagram (with $\log T_{\mathrm{eff}} \leq 3.8$) and are evolving along the Hayashi track up to the radiative phase of the PMS evolution. We are therefore convinced that the BM01 birthline is a reasonable assumption for the start of the PMS phase at all masses.

In Fig. 4 all the stars of our sample are plotted, with circles for non-magnetic stars, squares for magnetic stars and a triangle for the candidate magnetic star. The BM01 birthline and the CESAM ZAMS are also overplotted. We observe that two points (the open circles) are situated way outside of the theoretical limits of the PMS region (from the birthline to the ZAMS), even taking into account their error bars. For the two corresponding stars (HD 98922 and IL Cep) we are therefore not able to estimate their mass, radius and age using the CESAM theoretical tracks. For stars situated just below the ZAMS, we have estimated the ranges of the parameters covered by the intersection area between the error ellipse and the HR diagram, and took the middle values. For the four magnetic stars, HD 190073, HD 200775, HD 72106 and V380 Ori, we have adopted the masses and radii reported in the papers that describe their spectroscopic and magnetic analyses (Catala et al. 2007; Alecian et al. 2008a; Folsom et al. 2008; Alecian et al. 2009b). However, we have redetermined their ages as different birthlines were used in these papers.

This method takes into account neither the uncertainties in the metallicity (however, see Section 4.2), nor the choice of the birthline. The inferred masses, radii and ages are therefore approximate, but will be useful when considering comparisons between the stars themselves. The masses, radii and ages are summarized in Table 2. In the same table we also give the PMS duration for each star, and the predicted radius that each star will have once it reaches the ZAMS. Both have been calculated by assuming a mass-constant evolution for each star. The PMS duration has been computed from the birthline. In the case of HD 34282, we did not calculate the ZAMS radius and the PMS duration because our models are of solar metallicity. HD 98922 and IL Cep fall well outside of the HR diagram, even when the errors on their temperatures and luminosities are taken into account. Furthermore, no distance, accurate enough to estimate a luminosity with reasonable error bars, could be found for HD 250550. Therefore no age, mass, radius, ZAMS radius and PMS duration could be estimated for these stars.

5 THE LEAST-SQUARES DECONVOLUTION PROFILE ANALYSIS

5.1 The LSD method

In order to increase the S/N of our line profiles, we applied the LSD procedure to all spectra (Donati et al. 1997). This procedure combines the information contained in many metal lines of the spectrum, in order to extract the mean intensity (Stokes I) and polarized (Stokes V) line profiles. In Stokes I, each line is weighted according to its central depth, while in Stokes V the profiles are weighted according to the product of the central depth, wavelength and Landé factor. These parameters are contained in a 'line mask' derived from a synthetic spectrum corresponding to the effective temperature and gravity of the star given in Table 2. The construction of the line mask for each star involved several steps. First, we used Kurucz ATLAS 9 models (Kurucz 1993) to obtain generic masks of solar abundances, and of $T_{\mathrm{eff}}/\log g$ following the Kurucz models grid. Our masks contain only lines with intrinsic depths larger or equal to 0.1, which, according to the S/N of our data, is sufficient. We then excluded from the masks hydrogen Balmer lines, strong resonance lines and lines whose Landé factor is unknown. At this stage, the mask contains all predicted lines satisfying the initial assumption of the LSD procedure, i.e. a similar shape for all spectral lines considered in the procedure. In the following this mask will be

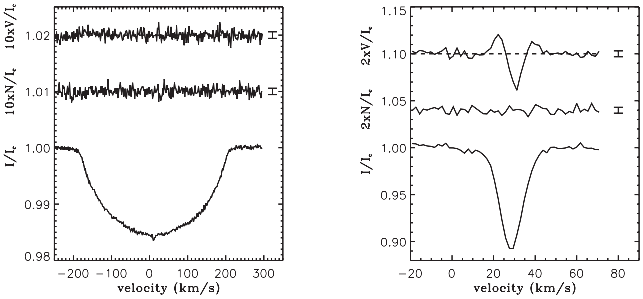

Figure 5. LSD Stokes *I* (bottom) and *V* (top) profiles of the non-magnetic Herbig Ae star 49 Cet (left) and the magnetic Herbig Ae star V380 Ori (right). The diagnostic *N* profile is also plotted in the middle. *V* and *N* have been shifted on the *Y*-axis, and magnified by a factor of 10 for 49 Cet and by a factor of 2 for V380 Ori, for display purposes.

called the 'full mask'. Finally, each mask was carefully examined in order to exclude lines predicted by the models, but not appearing in the spectrum, as well as lines contaminated by non-photospheric features. This final 'cleaning' procedure is explained in Section 5.2 and detailed for each star in Appendix A. Following this procedure, we executed LSD using the full and cleaned masks and the observed spectra, obtaining for each star the mean intensity Stokes *I* profile, the mean circularly polarized Stokes *V* profile and the null *N* profile. Fig. 5 shows the LSD *I*, *V* and *N* profiles for two stars: one with a magnetic field detection and one without. In both cases, as well as in all of our observations, the *N* profiles are null indicating the absence of spurious polarization signals, and confirming that the Zeeman signatures detected in the magnetic stars are real. The use of two separate masks per star is justified in the following sections. The analysis of the LSD *I* profile and the rotation velocity measurements are described in Section 5.2, while the magnetic analysis performed using the *I* and *V* profiles is detailed in Section 6.

The LSD method implies that all lines of the spectra have a similar shape, differing only in their relative strength. The strengths depend on the central depth when the method is applied to an *I* spectrum, and on the central depth and Landé factor for a polarized *V* spectrum. This hypothesis is reasonable for purely photospheric lines. However, in the case of a spectrum contaminated with CS features, these hypotheses should be discussed. The CS features contaminating the photospheric lines of the spectra of the Herbig Ae/Be stars have the same shape (except in few lines like the Balmer, Ca II H&K or Na D lines, which are removed from the mask). However, their relative strength is not dependent on the central depths of the photospheric lines, which are used to weight each line in the LSD procedure. Therefore, the LSD method, by averaging the contaminated lines, applies inappropriate weights to the CS contribution, while taking correctly into account the different weights of the photospheric lines. In the LSD procedure, using wrong weights does not change the global shape of the resulting profile; however, its relative strength (with respect to the *V* profile, for example) cannot be trusted. Therefore, the strength of the CS contribution of our LSD *I* profiles must be investigated in more detail before it can be reliably used to drawn any quantitative conclusions. However, its shape can be modelled and removed to be able to analyse the photospheric contribution of the *I* profile, which is one of the interests for this paper. We describe in the following section how the CS contamination has been handled in this study.

5.2 Fitting of the LSD *I* profiles

The LSD *I* profiles computed with the full mask reveal a rather complex average of the lines of the spectrum included in the line mask. Most HAeBe stars show CS emission and absorption in their spectrum; these effects are also reflected in the LSD profiles. Those lines that are most strongly contaminated by CS emission can be easily identified directly in the spectrum itself, and excluded from the mask. For some of the stars, the resulting LSD profiles show a relatively clean rotational profile indicative of simple photospheric absorption. For others, the resulting profiles still show significant CS absorption and/or emission that is not possible to remove by further refinement of the line mask. However, the investigations of rotation and magnetic fields in Papers II and III require that we are able to extract an approximation of the uncontaminated photospheric profiles in order to infer $v\sin i$ and to model the magnetic constraint imposed by Stokes *V*.

To characterize the various contributions to the LSD *I* profiles, we have performed a least-squares fit to each of the LSD *I* profiles using several models. In the first case we consider a simple photospheric profile modelled using the convolution of a rotation function (depending on the projected rotational velocity $v\sin i$ and the radial velocity of the star $v_{\rm rad}$), and a Gaussian (approximating the local photospheric profile) whose width is fixed and computed from the spectral resolution and the macroturbulent velocity (Gray 1992). This convolution will be called the photospheric function. The free parameters of the fitting procedure are the line depth, $v\sin i$ and $v_{\rm rad}$. In order to fit the wings of the observed LSD profiles of our sample, a macroturbulent velocity ($v_{\rm mac}$) is frequently required to be added to the model. Only a few stars of our sample have LSD *I* profiles suitable for estimating the value of $v_{\rm mac}$, and the typical value is found to be around 2 km s^{-1}. The other stars of our sample (i.e. most of them) display too large a Doppler broadening, and/or the wings of the profile are sufficiently contaminated by CS features, that they do not allow us to obtain useful information about $v_{\rm mac}$. Nonetheless, we assumed that a macroturbulent velocity field is present near the surface of the star, and we adopted for all the stars an isotropic macroturbulent velocity of 2 km s^{-1}. However, taking into account a $v_{\rm mac}\sim 2$ km s^{-1} seems to improve the fit, when fitting with the eye, only for stars with $v\sin i$ lower than 40 km s^{-1}. In order to estimate the error on the $v\sin i$ introduced by fixing $v_{\rm mac}$, we varied the value of $v_{\rm mac}$ between 0 and 4 km s^{-1}, and we find that it introduces significant variations of $v\sin i$ only if $v\sin i$ is lower than 10 km s^{-1}. For $v\sin i$ between 10 and 40 km s^{-1}, changing $v_{\rm mac}$ modifies the value of $v\sin i$ within the error bars. For $v\sin i$ larger than 40 km s^{-1}, changing $v_{\rm mac}$ has no impact on $v\sin i$. The macroturbulent velocity is therefore not a significant parameter to be considered within this fitting procedure. It has been included in all the fitted models for consistency from one star to the other, but should only be considered with caution at very low $v\sin i$ (lower than 10 km s^{-1}).

The second model considers one or more Gaussian functions meant to model the CS features present in the LSD *I* profile. These functions are added to the photospheric function with the aim of providing the best reproduction of the observed profile. The parameters of each Gaussian contributing to the CS function are the full width at half-maximum (FWHM), the centroid position and the amplitude. The amplitude may be either positive or negative, corresponding to emission or absorption contributions. Depending on the star analysed, we require between zero and four CS functions to fit the Stokes *I* profile. Hence, the number of fitting parameters required to reproduce the LSD *I* profiles ranges from 3 to 15.

For a few stars for which this simple model was unable to reproduce features in the observed profile, an alternative method we applied was to suppress from the fit the regions contaminated with CS (or other) features. We accomplished this by assigning a null weight to all points inside the affected region, and fit the profile with only a photospheric function.

The LSD profiles of our observations show systematically a continuum level lower than 1 (while the spectra are all normalized to 1). We believe that this is due to spectral features not taken into account in the LSD procedure, and not due to poor continuum normalization or to a reduction problem, for two reasons. First, multiple LSD profiles of a star obtained at different times show a continuum at the same level. However, multiple observations of different stars do not have the same continuum level, suggesting that the choice of the mask might determine the level of the continuum. Secondly, when we apply the LSD procedure on a simulated ESPaDOnS or Narval observation, in which the continuum is by construction perfectly normalized to 1, the continuum level of the resulting *I* profile is also lower than 1.

In order to simplify the fitting procedure and avoid additional parameters to fit, we have normalized each profile before fitting them. The continuum levels have been determined by fitting a line between two points chosen by eye on each side of the profiles. The profiles are then divided by the fitted continuum. We have checked that this normalization process does not introduce significant errors by repeating the procedure many times and checking that the fitted parameters converge all towards the same value.

A remarkable result of this procedure is the conclusion that the mean line profiles of most HAeBe stars can be satisfactorily reproduced by a simple model consisting of the sum of a rotationally broadened photospheric profile and a small number of local absorption/emission profiles assumed to be contributed by the CS environment. The analysis of the quantitative characteristics of the CS-contributed profiles will be described in a future paper.

As an additional complication, some stars in our sample are double-lined spectroscopic binaries (see Section 5.3). In these cases, we fitted the LSD *I* profiles using the sum of two photospheric functions, each one having independent fitting parameters. Examples of the results of the fitting procedure are shown in Fig. 6.

This fitting procedure is automatic and requires as input first guesses for each free parameter. We checked the uniqueness of the derived fit by modifying the first guesses, and checking that whatever the first guesses, the fits always converge towards a unique solution. This verification procedure was always successful for the photospheric parameters (the photospheric line depth, $v \sin i$ and $v_{\rm rad}$). However, in some cases when one or more Gaussian CS functions was required, we could find multiple solutions (e.g. the addition of a Gaussian in emission or a Gaussian in absorption could give fits of comparable quality). In those cases we checked individual spectral lines in order to determine which of the solutions was the most consistent with the observed spectrum. Whenever multiple observations were obtained for the same star, we also chose the solution the most consistent over all observations.

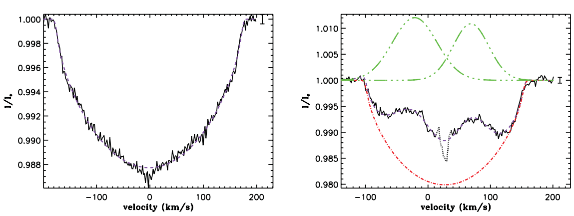

Figure 6. Examples of LSD fits (dashed purple line) using only a photospheric (red dot–dashed line) function for HD 176386 (left) and using a photospheric + two Gaussian (green dot-dot-dot–dashed line) functions for HD 36917 (right) observed on 2007 November 8. In the case of HD 36917, the narrow absorption in the core of the profile (dotted line) has been excluded from the fit.

When multiple observations were obtained for the same star with similar S/N values, we performed a simultaneous fit to the whole set of observations, by forcing the photospheric parameters (depth, $v \sin i$, $v_{\rm rad}$) to be the same for each of the observations. When necessary, one or more Gaussian functions were added to the profiles, with independent parameters for each observation.

We checked that changing the effective temperature and gravity of the masks, within the error bars, do not change our determination of our $v \sin i$ values. The fit performed to reproduce the shape of the LSD *I* profile is dominating the uncertainties. The uncertainties on the adopted parameters (see Table 2) have therefore been determined by calculating the confidence intervals at a level of 99.73 per cent, as described in Press et al. (1992, p. 697).

After completing the analysis of the LSD profiles, we checked that the derived $v \sin i$ were consistent with individual spectral lines in the reduced spectra. The adopted values of $v \sin i$ and $v_{\rm rad}$ are summarized in Table 2, and the fitting procedure for each of the spectra is described in Appendix A. In the case of MWC 1080, no photospheric lines could be identified in the spectrum, therefore no $v \sin i$ values could be measured.

5.3 The discovery of spectroscopic binaries

The inspection of the LSD profiles allowed us to easily identify a number of spectroscopic binaries among the stars in our sample. Among the stars not detected as magnetic, a total of five SB2 systems were identified: three previously known or suspected (AK Sco, HD 287823, IL Cep), and two new discoveries previously unreported in the literature (HD 203024 and HD 290409). Based on the detection of a LiI lines at 6707 A, Corporon & Lagrange (1999) claimed the presence of a low-mass companion orbiting HD 203024. However, this claimed companion cannot be the spectroscopic companion that we detect because its temperature is too high. We therefore cast some doubts on the stellar nature of the feature observed at ∼6708 Å, and leave open the interpretation of its origin.

For each of the SB2 systems, we have attempted a determination of the effective temperature of both components, as well as of their luminosity ratio. The description of each system is detailed in Appendix A.

6 MAGNETIC FIELD DIAGNOSIS

6.1 Method

Each of the spectra that we have acquired with ESPaDOnS and Narval was obtained in Stokes *V* polarimetric mode, in order to allow us to measure the longitudinal Zeeman effect in spectral lines. We employ two methods to detect magnetic fields in our program and standard stars. First, we use the Stokes *V* spectra to measure the mean longitudinal magnetic field strength $\langle B_z \rangle$ of each star at the time of observation. This is the conventional measure of field strength normally used for detection of magnetic fields in MS stars (e.g. Landstreet 1982). However, because of the high value of the resolving power, we can also examine spectral lines for the presence of circular polarization signatures: Zeeman splitting combined with Doppler broadening of lines by rotation leads to non-zero values of V within spectral lines even when the value of $\langle B_z \rangle$ is close to, or even equal to, zero. This possibility substantially increases the sensitivity of our measurements as a discriminant of whether a star is in fact a magnetic star or not, as discussed by Shorlin et al. (2002), Silvester et al. (2009) and Shultz et al. (2012).

Each set of LSD Stokes I and V profiles is therefore analysed in two ways. First, the value of $\langle B_z \rangle$ is determined by computing the first-order moment of Stokes V, normalized to the equivalent width of Stokes I (Mathys 1991; Donati et al. 1997; Wade et al. 2000):

$$\langle B_z \rangle = -2.14 \times 10^{11} \frac{\int v V(v)\, \mathrm{d}v}{\lambda \bar{g} c \int [I_c - I(v)]\, \mathrm{d}v}, \tag{1}$$

where $\langle B_z \rangle$ is in G, $\bar{g}$ is the mean Landé factor of the LSD weights in the line mask (typically 1.3 ± 0.1) and λ is the S/N-weighted mean wavelength of the LSD weights in the mask in nm (typically 520 ± 40 nm). The uncertainties σ on $\langle B_z \rangle$ have been computed by propagating the error of each pixel within the Stokes I and V profiles through equation (1). The limits of integration are usually chosen for each star to coincide with the observed limits of the LSD I and V profiles; using a smaller window would neglect some of the signal coming from the limb of the star, while a window larger than the actual line would increase the noise without adding any further signal, thus degrading the S/N below the optimum value achievable (see e.g. Neiner et al. 2012).

In addition, the LSD Stokes V profile is itself examined. We evaluate the false alarm probability (FAP) of V/I_c inside the line according to

$$\mathrm{FAP}\,(\chi_r^2, \nu) = 1 - P\left(\frac{\nu}{2}, \frac{\nu \chi_r^2}{2}\right), \tag{2}$$

where P is the incomplete gamma function, ν is the number of spectral points inside the line and χ_r^2 is the reduced chi square (χ^2/ν) computed across the V profile relative to zero (e.g. Donati, Semel & Rees 1992). The FAP value gives the probability that the observed V signal inside the spectral line could be produced by chance if there is actually no field present. Thus a very small value of the FAP implies that a field is actually present. We evaluate FAP using the detection thresholds of Donati et al. (1997). We consider that an observation displays a 'definite detection' (DD) of Stokes V Zeeman signature if the FAP is lower than 0.000 01, a 'marginal detection' (MD) if it falls between 0.001 and 0.000 01, and a 'null detection' (ND) otherwise. As mentioned above a *significant signal* (i.e. with a MD or DD) may occur even if $\langle B_z \rangle$ is not significantly different from zero. In contrast, a profile can give a $\langle B_z \rangle$ different from zero at a level of 3σ or lower without displaying a marginal or a definite detection (see Fig. 10 and Section 6.3). For these reasons, the FAP is the most sensitive diagnostic of the presence of a magnetic field, and will be the only one applied in this paper. Table 4 summarizes our measurements of FAP and the magnetic diagnosis (DD, MD or ND) for all observations, except those already published in previous papers.

If a significant signal (i.e. with a MD or DD) is detected within the line, while always remaining insignificant in the neighbouring continuum and in the N profile, and is detected in multiple observations, we conclude that the star is unambiguously magnetic.

6.2 The magnetic HAeBe stars detected within the survey

Of the 70 stars observed with ESPaDOnS and Narval, six show Stokes V Zeeman signatures in their LSD profiles. Four of these stars (V380 Ori, HD 72106, HD 190073 and HD 200775) were unambiguously detected for the first time as a result of this study. First results for V380 Ori and HD 72106 were reported by Wade et al. (2005); for HD 190073 by Catala et al. (2007); and for HD 200775 by Alecian et al. (2008a). In addition, one HAeBe star for which magnetic field detections were previously reported (HD 36982 = Par 1772 = LP Ori ; Petit et al. 2008) is confirmed to be magnetic. Finally, one new suspected magnetic HAeBe star (HD 35929) is reported here. However, as HD 35929 is a δ-Scuti pulsating star (Marconi et al. 2000), more analysis and observations are required to verify that the signature detected in the V profile is of magnetic origin.

Table 3. Log of our first observations of HAeBe stars in which we have detected a magnetic field. Column 1 gives the name of the star. Columns 2–4 report the Heliocentric Julian Date, the type of detection (MD for marginal detection and DD for definite detection) and the longitudinal field measurement reported in the literature. In the final column we indicate the first refereed publication in which the field detection was reported. Discoveries by Wade et al. (2005), Catala et al. (2007) and Alecian et al. (2008a) are derived from this survey. LP Ori was reported to be magnetic by Petit et al. (2008) as part of a parallel program. However, as it was serendipitously detected within this survey as well, we include this star as a *bona fide* blind detection in our statistics.

Name	HJD − 245 0000	Det	$\langle B_z \rangle \pm \sigma_B$ (G)	Discovery paper
		Confirmed magnetic HAeBe stars		
V380 Ori	3421.900	MD	-165 ± 190	Wade et al. (2005)
HD 36982	4416.549	MD	-240 ± 70	Petit et al. (2008)
HD 72106	3423.924	DD	228 ± 50	Wade et al. (2005)
HD 190073	3607.789	DD	111 ± 13	Catala et al. (2007)
HD 200775	3608.920	MD	74 ± 63	Alecian et al. (2008a)
		Suspected magnetic HAeBe stars		
HD 35929	4884.328	DD	74 ± 19	This paper

In Table 3, for each of the detected program stars, we list the observational details corresponding to the ESPaDOnS/Narval observations from which the presence of a magnetic field was first inferred. In addition, in Fig. 4 we show the positions on the HR diagram of the magnetic HAeBe stars of our sample.

Each of the five detected stars has been or will be discussed in detail in a dedicated paper (e.g. HD 190073 by Catala et al. 2007, HD 200775 by Alecian et al. 2008a, HD 72106 by Folsom et al. 2008 and V380 Ori by Alecian et al. 2009b). They will not be discussed further here.

Five other magnetic HAeBe stars have been discovered and confirmed during recent years, as part of parallel observational programs with ESPaDOnS, Narval and FORS1 on the Very Large Telescope (ESO, Chile), or the Semel Polarimeter (SEMPOL; Semel 1989; Semel, Donati & Rees 1993; Donati et al. 2003) coupled with the spectrograph UCLES on the Anglo Australian Telescope (AAT, Australia). The first magnetic detections and their confirmations are reported or are to be reported in other publications: HD 101412 (Wade et al. 2007; Hubrig et al. 2009; Paper IV), HD 104237 (Donati et al. 1997; Paper IV), NGC 6611 601 (Alecian et al. 2008b), NGC 2244 201 (Alecian et al. 2008b) and NGC 6611 83 (Alecian et al. 2009a). We are mentioning them in this paper for the sake of completeness; however, they will not be included in the statistical analyses that will be presented in Papers II and III as they are not part of the survey presented in this series of papers. They will not be discussed any further here.

Table 4. Results of the magnetic analysis of the program HAeBe stars. The data of HD 190073, V380 ori, HD 200775 and HD 72106 have already been published and do not appear here. Columns 1 and 2 give the name of the star and the date of the observation. Columns 3 and 4 give the limits of the integration range. The false alarm probability (FAP) of a Zeeman detection in the V profile is indicated in column 5. The magnetic diagnosis (ND, MD or DD) is indicated in column 6. The B_ℓ measurement, its error (σ) and the detection significance (B_ℓ/σ) computed using the hybrid and original profiles are given in the columns 7–10. The final column give the ratio of the B_ℓ errors of the hybrid over the observed solutions.

Filename	Date	Start (km s^{-1})	End (km s^{-1})	FAP	Diagnosis	Hybrid $B_\ell \pm \sigma$ (G)	Hybrid B_ℓ/σ	Original $B_\ell \pm \sigma$ (G)	Original B_ℓ/σ	$\sigma_{\rm syn}/\sigma_{\rm obs}$
BD−06 1259	12/03/09	−25	69	0.7990	ND	62 ± 87	0.711	37 ± 51	0.711	1.71
	20/02/05	−25	69	0.5826	ND	53 ± 54	0.986	31 ± 31	0.987	1.74
BD−05 1329	23/08/05	−148	205	0.6266	ND	201 ± 396	0.508	144 ± 282	0.508	1.40
BD−05 1324	11/01/06	−59	118	0.3831	ND	−51 ± 111	−0.455	−47 ± 103	−0.455	1.08
BD+41 3731	06/11/07	−428	400	1.0000	ND	2367 ± 1890	1.252	3415 ± 2731	1.250	0.69
	25/08/05	−428	400	0.9987	ND	50 ± 1008	0.049	51 ± 1038	0.049	0.97
BD+46 3471	25/08/05	−242	235	0.6788	ND	−20 ± 526	−0.038	−45 ± 1202	−0.038	0.44
BD+61 154	21/02/05	−151	118	0.6030	ND	146 ± 666	0.219	−16 ± 74	−0.219	9.00
	23/08/05	−151	118	0.2323	ND	985 ± 549	1.796	−177 ± 98	−1.798	5.60
BD+65 1637	10/06/06	−360	308	0.9998	ND	574 ± 1109	0.518	−2045 ± 3955	−0.517	0.28
	24/09/09	−360	308	0.9997	ND	−806 ± 874	−0.923	938 ± 1023	0.917	0.85
BD+72 1031	11/06/06	−59	118	0.9309	ND	−28 ± 118	−0.234	−36 ± 156	−0.234	0.76
	11/11/07	−225	207	0.9810	ND	1072 ± 1122	0.955	412 ± 431	0.956	2.60
HD 9672	24/08/05	−221	247	0.9509	ND	27 ± 111	0.239	27 ± 111	0.239	1.00
HD 17081	19/02/05	−11	37	0.3758	ND	2 ± 7	0.268	2 ± 8	0.268	0.88
	20/02/05	−13	35	0.9972	ND	0 ± 7	0.010	0 ± 7	0.010	1.00
HD 31293	27/11/04	−113	163	0.5567	ND	−112 ± 87	−1.283	393 ± 308	1.274	0.28
	19/02/05	−113	163	0.8017	ND	−27 ± 157	−0.172	31 ± 179	0.172	0.88
	21/02/05	−113	163	0.7151	ND	51 ± 103	0.490	−63 ± 128	−0.490	0.80
HD 31648	21/02/05	−104	130	0.9268	ND	9 ± 65	0.134	10 ± 77	0.134	0.84
	24/08/05	−104	130	0.9687	ND	149 ± 62	2.411	220 ± 92	2.408	0.67
HD 34282	24/08/05	−111	142	0.3744	ND	−223 ± 148	−1.505	−369 ± 246	−1.504	0.60
HD 35187 B	25/08/05	−85	139	0.7977	ND	−94 ± 101	−0.925	−86 ± 93	−0.926	1.09
HD 35929	11/03/09	−53	95	0.9993	ND	−8 ± 35	−0.227	−6 ± 28	−0.227	1.25
	12/11/07	−53	95	0.0091	ND	−59 ± 23	−2.598	−45 ± 17	−2.598	1.35
	13/11/07	−53	95	0.9704	ND	−137 ± 45	−3.007	−106 ± 35	−3.007	1.29
	20/02/09	−53	95	0.0002	MD	33 ± 17	1.957	25 ± 13	1.957	1.31
	21/02/09	−53	95	0.0000	DD	74 ± 19	3.928	57 ± 15	3.928	1.27
HD 36112	29/11/04	−47	83	0.9382	ND	27 ± 26	1.034	26 ± 25	1.034	1.04
	19/02/05	−47	83	0.9395	ND	−35 ± 33	−1.059	−33 ± 31	−1.059	1.06
HD 36910	04/04/08	−81	143	0.9018	ND	−141 ± 85	−1.654	−180 ± 109	−1.653	0.78
HD 36917	08/11/07	−126	179	0.9960	ND	−672 ± 384	−1.748	−978 ± 560	−1.745	0.69
HD 36982	08/11/07	−65	90	0.9402	ND	−307 ± 251	−1.224	−326 ± 267	−1.224	0.94
	09/11/07	−65	90	0.0059	ND	−225 ± 108	−2.090	−227 ± 109	−2.086	0.99
	10/11/07	−65	90	1.0000	ND	−10 ± 79	−0.129	−10 ± 76	−0.129	1.04
	11/11/07	−65	90	0.0009	MD	−248 ± 76	−3.267	−233 ± 71	−3.265	1.07
HD 37258	24/02/09	−209	271	0.6827	ND	−216 ± 404	−0.535	−196 ± 366	−0.535	1.10
HD 37357	24/02/09	−127	170	0.9917	ND	133 ± 197	0.674	212 ± 315	0.674	0.63
HD 37806	24/08/05	−97	191	0.1909	ND	239 ± 179	1.336	349 ± 261	1.334	0.69
HD 38120	13/03/09	−89	144	0.3659	ND	191 ± 203	0.942	679 ± 723	0.939	0.28
HD 38238	16/03/07	−105	133	0.7370	ND	18 ± 81	0.221	20 ± 90	0.221	0.90
HD 50083	03/04/08	−279	278	0.9978	ND	124 ± 236	0.525	10860 ± 33614	0.323	0.01
	12/11/07	−279	278	1.0000	ND	−229 ± 191	−1.200	−304 ± 254	−1.200	0.75
HD 52721	03/04/08	−237	280	0.9520	ND	222 ± 235	0.943	212 ± 225	0.943	1.04
	06/11/07	−237	280	1.0000	ND	−22 ± 204	−0.107	−24 ± 220	−0.107	0.93
HD 53367	19/02/05	−2	97	0.9606	ND	−19 ± 46	−0.406	−20 ± 48	−0.406	0.96
	20/02/05	−2	97	0.9917	ND	18 ± 29	0.617	19 ± 31	0.617	0.94
HD 68695	21/02/05	−32	73	0.7696	ND	10 ± 125	0.078	15 ± 188	0.078	0.66
HD 76534 A	21/02/05	−58	105	0.9331	ND	−154 ± 151	−1.019	−203 ± 199	−1.019	0.76
HD 98922	20/02/05	−60	60	0.3729	ND	−144 ± 71	−2.015	194 ± 96	2.012	0.74
HD 114981	11/01/06	−335	236	0.9968	ND	−105 ± 203	−0.518	−157 ± 303	−0.518	0.67
	19/02/05	−335	236	0.9875	ND	−117 ± 459	−0.255	−197 ± 775	−0.255	0.59
HD 135344	09/01/06	−98	98	0.9417	ND	−124 ± 138	−0.893	−131 ± 147	−0.893	0.94
HD 139614	19/02/05	−29	29	0.1845	ND	−24 ± 14	−1.760	−22 ± 12	−1.760	1.17
	20/02/05	−29	29	0.8027	ND	−13 ± 14	−0.947	−11 ± 12	−0.947	1.17
	21/02/05	−29	29	0.7707	ND	12 ± 12	0.998	11 ± 11	0.998	1.09

Table 4 – *continued*

Filename	Date	Start (km s^{-1})	End	FAP	Diagnosis	Hybrid $B_\ell \pm \sigma$ (G)	Hybrid B_ℓ/σ	Original $B_\ell \pm \sigma$ (G)	Original B_ℓ/σ	$\sigma_{\rm syn}/\sigma_{\rm obs}$
HD 141569	06/03/07	−286	262	0.6638	ND	−73 ± 149	−0.492	−591 ± 1219	−0.485	0.12
	12/02/06	−286	262	0.8590	ND	645 ± 778	0.829	1672 ± 2023	0.826	0.38
HD 142666	19/02/05	−85	72	0.9918	ND	28 ± 78	0.359	22 ± 60	0.359	1.30
	21/02/05	−85	72	0.4443	ND	−45 ± 44	−1.009	−34 ± 34	−1.010	1.29
	21/05/05	−85	72	0.8100	ND	16 ± 53	0.298	12 ± 39	0.298	1.36
	21/05/05	−85	72	0.9985	ND	−29 ± 53	−0.543	−21 ± 39	−0.543	1.36
	22/05/05	−85	72	0.6419	ND	54 ± 62	0.873	39 ± 45	0.873	1.38
	23/05/05	−85	72	0.8755	ND	−14 ± 50	−0.282	−11 ± 37	−0.282	1.35
	24/05/05	−85	72	0.5239	ND	−29 ± 56	−0.511	−21 ± 42	−0.511	1.33
HD 144432	19/02/05	−97	93	0.7430	ND	−113 ± 49	−2.296	−101 ± 44	−2.296	1.11
	20/02/05	−97	93	0.8485	ND	−9 ± 41	−0.227	−8 ± 36	−0.227	1.14
HD 144668	23/08/05	−249	229	0.8869	ND	299 ± 145	2.064	191 ± 92	2.066	1.58
HD 145718	25/08/05	−139	132	0.0961	ND	17 ± 85	0.204	15 ± 72	0.204	1.18
HD 150193	23/08/05	−135	125	0.8757	ND	−194 ± 117	−1.664	−382 ± 230	−1.661	0.51
HD 163296	21/05/05	−164	146	0.8992	ND	41 ± 106	0.387	103 ± 266	0.387	0.40
	22/05/05	−164	146	0.9703	ND	47 ± 141	0.333	59 ± 176	0.333	0.80
	23/05/05	−164	146	0.7855	ND	138 ± 96	1.431	160 ± 112	1.431	0.86
	23/05/05	−164	146	0.8324	ND	0 ± 135	−0.001	0 ± 131	−0.001	1.03
	24/05/05	−164	146	0.6017	ND	109 ± 96	1.134	250 ± 221	1.132	0.43
	24/05/05	−164	146	0.6782	ND	313 ± 136	2.292	523 ± 229	2.285	0.59
	24/08/05	−164	146	0.2564	ND	202 ± 93	2.160	−1835 ± 998	−1.840	0.09
HD 169142	19/02/05	−58	57	0.9872	ND	12 ± 28	0.434	23 ± 52	0.434	0.54
	21/02/05	−58	57	0.1944	ND	51 ± 34	1.521	100 ± 66	1.520	0.52
	21/05/05	−58	57	0.9848	ND	−21 ± 20	−1.038	−40 ± 38	−1.038	0.53
	23/08/05	−58	57	0.9943	ND	28 ± 12	2.215	52 ± 23	2.214	0.52
HD 174571	15/04/08	−249	277	0.9923	ND	−1733 ± 687	−2.521	−1825 ± 724	−2.520	0.95
	16/03/07	−249	277	0.9983	ND	213 ± 544	0.392	220 ± 560	0.392	0.97
HD 176386	24/08/05	−212	208	0.6676	ND	304 ± 239	1.272	309 ± 243	1.271	0.98
HD 179218	03/10/09	−67	98	0.9902	ND	−1 ± 39	−0.026	−1 ± 42	−0.026	0.93
	20/02/05	−67	98	0.3448	ND	−97 ± 114	−0.850	−98 ± 115	−0.849	0.99
	25/08/05	−67	98	0.8626	ND	77 ± 50	1.536	78 ± 51	1.536	0.98
HD 244314	05/11/07	−40	85	0.9511	ND	−46 ± 106	−0.436	−39 ± 90	−0.436	1.18
HD 244604	23/08/05	−91	145	0.8532	ND	−90 ± 79	−1.138	−103 ± 91	−1.137	0.87
HD 245185	19/02/05	−124	157	0.7352	ND	−255 ± 335	−0.760	−1674 ± 2216	−0.755	0.15
HD 249879	05/04/08	−294	316	0.9577	ND	1465 ± 1326	1.104	971 ± 879	1.104	1.51
HD 250550	07/11/07	−117	72	0.0256	ND	−60 ± 249	−0.241	54 ± 225	0.241	1.11
HD 259431	17/03/07	−73	126	0.7920	ND	−117 ± 184	−0.636	75 ± 118	0.636	1.56
	17/03/10	−73	126	0.3502	ND	22 ± 281	0.078	−27 ± 351	−0.078	0.80
	24/02/09	−73	126	0.6835	ND	93 ± 197	0.474	−58 ± 122	−0.474	1.61
HD 275877	10/12/06	−267	270	0.9871	ND	80 ± 303	0.263	43 ± 163	0.263	1.86
	24/09/09	−267	270	0.9182	ND	6 ± 418	0.014	5 ± 346	0.014	1.21
HD 278937	20/02/05	−82	109	0.8934	ND	74 ± 119	0.627	81 ± 129	0.627	0.92
	20/02/05	−82	109	0.7830	ND	−105 ± 147	−0.717	−113 ± 158	−0.717	0.93
	21/02/05	−82	109	0.9398	ND	−62 ± 166	−0.370	−67 ± 180	−0.370	0.92
HD 287841	20/02/09	−119	159	0.7004	ND	61 ± 268	0.229	55 ± 242	0.229	1.11
HD 290409	06/11/07	−299	301	0.9883	ND	−939 ± 980	−0.958	−4140 ± 4385	−0.944	0.22
HD 290500	21/02/09	−73	131	0.9775	ND	601 ± 464	1.296	557 ± 430	1.295	1.08
HD 290770	24/02/09	−249	324	0.8890	ND	1088 ± 985	1.105	2264 ± 2068	1.095	0.48
HD 293782	10/01/06	−253	277	0.8452	ND	1178 ± 942	1.251	508 ± 406	1.253	2.32
HD 344261	06/11/07	−240	231	0.9608	ND	−817 ± 928	−0.880	−463 ± 526	−0.880	1.76
	23/08/05	−240	231	0.7389	ND	−275 ± 491	−0.561	−162 ± 289	−0.561	1.70
VV Ser	25/08/05	−100	201	0.9998	ND	1138 ± 485	2.348	561 ± 238	2.355	2.04
VX Cas	/24/08/05	−199	180	0.9707	ND	−286 ± 994	−0.288	−242 ± 840	−0.288	1.18

6.3 Magnetic analysis of the remaining sample

The polarized spectra of the undetected stars, i.e. displaying no magnetic signatures, contain a valuable information that we want to extract: the upper limits on admissible surface magnetic fields. In this section we first describe the problems that a typical spectrum of Herbig Ae/Be stars can bring in evaluating realistic values of such limits due to the CS contribution to the spectra. Then we propose the method that we adopted to solve the problems: the hybrid method.

6.3.1 The CS contribution to the Stokes I and V spectra

Before discussing the analysis of the stars in which no firm magnetic detections was obtained, it is instructive to consider the formation of the stellar spectrum, beginning in the photosphere of a magnetized HAeBe star. Upon exiting the 'top' of the photosphere, the (absorption) lines will be partially circularly polarized due the magnetic field. As the flux propagates into the CS environment, it will undergo absorption or emission contributions due to the CS material. As observed in the spectra of real HAeBe stars, this can strongly modify the Stokes *I* line profiles. However, we expect that the magnetic field strength will decrease rapidly with distance from the star as $1/r^3$ for a dipole, and more rapidly for more complex fields. Therefore the contribution of the Zeeman effect to Stokes *V* in the CS environment should be very small compared to the photospheric contribution. In other words, the CS contribution to the flux is expected to be negligibly circularly polarized. A consequence of this conclusion is that the observed Stokes V/I_c spectrum of a magnetic HAeBe star is expected to be reflective of the *photospheric* spectrum of the star, even if the Stokes *I* spectrum is strongly modified by the CS environment. An important implication of this conclusion it that CS contamination of spectral lines cannot serve to 'hide' the Zeeman signatures produced by a photospheric magnetic field. Note, however, that because the *V* spectrum is normalized to the inferred continuum, this conclusion and its implication rely on the assumption that no significant veiling is present (Ghandour et al. 1994; Folsom et al. 2012). Although veiling does not modify the absolute amplitude or shape of the Zeeman signature, it serves to increase the noise, and could therefore render a Zeeman signature undetectable.

The LSD profiles produced for line profile analysis in Section 5.2 with the cleaned masks are heavily filtered: many lines have been removed from the line masks in order to reduce the CS contribution and to reveal the photospheric profile. In the case of the Stokes *V* profile, this results in a relatively high noise level (because of the relatively small number of lines used in the deconvolution) and consequently low sensitivity to magnetic fields (see the S/N in *V* obtained from both full and cleaned masks in Table 1). However, in contrast to the Stokes *I* profile, we have concluded that Stokes *V* is not strongly modified by the CS contribution to the line. Therefore the most sensitive magnetic diagnosis should be obtained by including as many lines as possible in the mask. However, as we have seen in Section 5, LSD Stokes *I* profiles derived from such masks can be heavily modified by CS contributions. Even if the Stokes *V* Zeeman signature is not modified significantly, using such contaminated *I* profiles has two important consequences for our diagnosis of the magnetic field. First, uncertainty is introduced into the appropriate integration range to use to compute the longitudinal magnetic field in equation (1), and the reduced χ^2 in equation (2). Secondly, the equivalent width of the Stokes *I* profile (i.e. the denominator of equation 1) is modified. Both of these consequences can change the inferred values of the longitudinal field and its error bar, while the first can influence the derived FAP. Of these, the impact on the longitudinal field is the most severe. For example, CS emission/absorption superimposed with the photospheric spectral lines can reduce/increase the equivalent with of the Stokes *I* profile significantly, artificially increasing/decreasing the derived longitudinal field and its error. In the absence of a magnetic detection, the longitudinal field error bar is the only important statistical quantity, as it provides an estimate of the upper limit on admissible fields. Because it is sensitive to CS contamination of Stokes *I*, it is important to understand, and potentially limit, the CS contribution to the *I* profile (even if the *V* profile is unmodified).

6.3.2 A hybrid approach

With these insights, we approached the problem of obtaining realistic quantitative longitudinal field measurements of the 65 program stars for which no significant magnetic field was detected. Our goal was to obtain measurements of the longitudinal field for which the error bars were simultaneously accurate and precise. The first option considered was to use the cleaned line masks described in Section 5. These have the advantage that they reveal, in many cases, the photospheric profile of the star. The disadvantage is that, in many cases, this is accomplished by excluding most of the lines – especially strong lines – that contribute significantly to reducing the Stokes *V* noise level. The second option was to use the full line masks. This has the advantage of reducing the noise level of Stokes *V* to the greatest extent, but the disadvantages of a strongly contaminated *I* profile (as described above). We considered using masks for which an intermediate level of cleaning had been applied, but it was not obvious to what extent to clean the masks, nor was it clear that we were not simply combining the uncertainties and disadvantages of both options 1 and 2.

In reality, we wished to combined the *advantages* of options 1 and 2, essentially by combining the more nearly photospheric Stokes *I* profiles obtained from the cleaned masks and the high-S/N Stokes *V* profiles from the full masks. While such an approach can solve the problem of determination of the integration range, it does not solve the problem of determination of the longitudinal field: the *I* and *V* profiles obtained from two different masks correspond to averages of different lines with different weights, and are therefore not directly comparable or quantitatively compatible in equation (1).

As a solution to this problem, we decided to take advantage of the atmospheric and spectral parameters determined in Sections 4 and 5 and to compute the approximate photospheric spectrum of each star using spectrum synthesis. We used the SYNTH3 LTE spectrum synthesis code (Kochukhov 2007) and effective temperature, surface gravity, $v \sin i$ and $v_{\rm rad}$ of each star (reported in Table 2) to compute its photospheric Stokes *I* spectrum with the same spectral domain and resolution as ESPaDOnS/Narval. We assumed solar abundances. To each synthetic spectrum we added synthetic Gaussian noise (calculated from the S/N of the spectra) that varied with wavelength in the same manner as in the observed spectrum. For each observed spectrum we then used the full line mask appropriate to the star to extract the Stokes *I* LSD profile from the synthetic spectrum, and the Stokes *V* LSD profiles from the observed spectrum. Combining the *I* and *V* profiles, this ultimately resulted in 'hybrid' LSD profiles consisting of the real, observed Stokes *V* profiles and a synthetic Stokes *I* profile, both extracted using the same mask. The advantage of this approach is that we avoid the uncertainty related to CS contributions to the Stokes *I* profile. On the other hand, we introduce uncertainty related to the compatibility of the synthetic photospheric spectrum with the real stellar photospheric spectrum.

6.3.3 Tests and effectiveness of the hybrid method

Using an integration range equal to the 1.2 times the measured $v \sin i$ of each star symmetric about the measured radial velocity, we evaluated equations (1) and (2) for each of the hybrid LSD profiles. For comparison, we also performed the same measurements, but using the original LSD profiles extracted using the full masks obtained only from the observed spectra. These measurements are listed in Table 4.

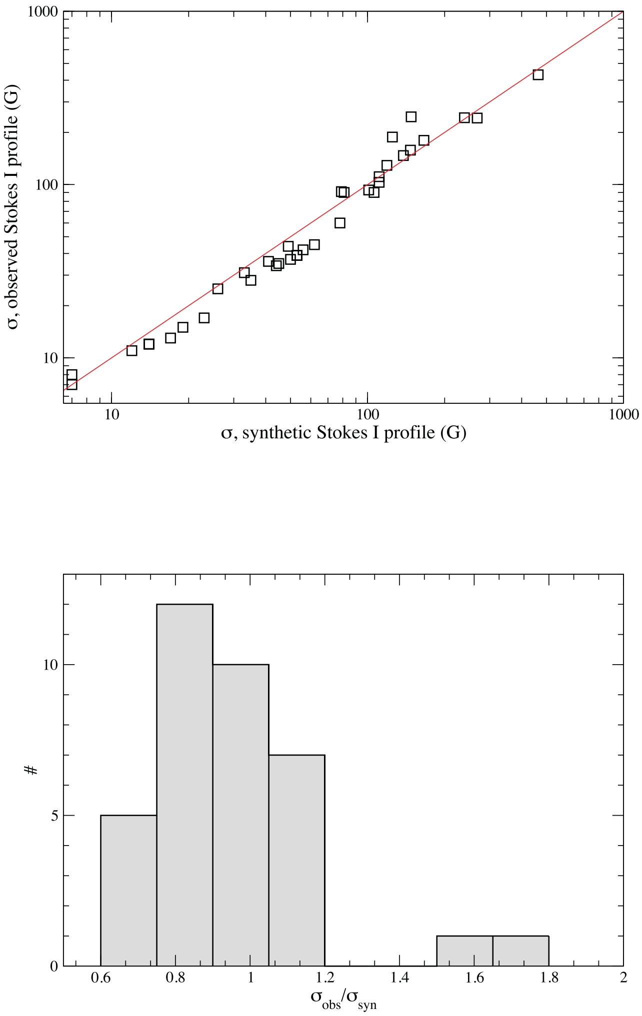

Figure 7. Comparison of longitudinal field error bars for synthetic versus observed Stokes *I* profiles. Upper panel: scatter plot of longitudinal field error bars computed using synthetic Stokes *I* versus error bars computed using the observed Stokes *I* dominated by the photospheric component only. The full (red) line corresponds to perfect agreement. Lower panel: histogram of the ratio of error bars with synthetic Stokes *I* to error bars with observed Stokes *I*, for observations with LSD profiles dominated by the photospheric component.

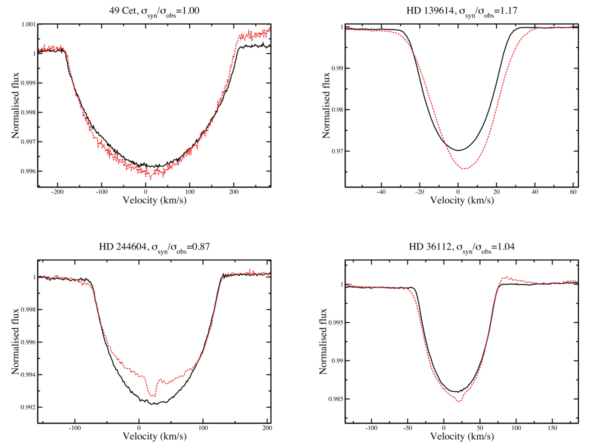

Figure 8. Illustrations of observed versus synthetic LSD Stokes *I* profiles for stars with profiles dominated by the photospheric component. The black full line is the synthetic, and the red dashed line is the observed. Upper left: 49 Cet. Upper right: HD 139614. Lower left: HD 244604. Lower right: HD 36112.

Based on the analysis of Section 5, we conclude that some of our observations have relatively small CS contamination, and are dominated by the photospheric component. We identified 17 stars (corresponding to 35 observations) for which this was the case; these stars are underlined in Table 4. We have used these observations as a test of the accuracy of this method by comparing the longitudinal field extracted using the LSD profiles with observed Stokes *I* profile, and those with the synthetic Stokes *I* profile. For stars with purely photospheric spectra we expect the longitudinal field error bars to agree. (Because the value of the longitudinal field itself is determined by the details of the noise pattern, we do not expect those values to agree, except that they should have values compatible with the uncertainties.) The results of this comparison are shown in Fig. 7.

The upper panel of Fig. 7 shows the derived value of the longitudinal field error bar using the synthetic Stokes *I* profile ($\sigma_{\rm syn}$, on the horizontal axis) versus that derived from the real Stokes *I* profile ($\sigma_{\rm obs}$, on the vertical axis) of the stars with mostly photospheric spectra. As can be seen, the correspondence between the error bars is quite close, with most points clustered tightly about the line $x = y$. The detailed agreement is summarized in the lower panel, which shows a histogram of the ratio $\sigma_{\rm syn}/\sigma_{\rm obs}$. The median of the distribution is 0.85, the mean is 1.2 and the standard deviation is 0.4. Most of the values of $\sigma_{\rm syn}/\sigma_{\rm obs}$ are clustered within ± 0.15 of unity, although two significant outliers (the stars HD 34282 and HD 68695) exist at $\sim$1.5. The dispersion results from (usually) small differences in the equivalent widths of the computed versus observed Stokes *I* profiles. A comparison of the observed and computed Stokes *I* profiles for four of the stars with mostly photospheric spectra is shown in Fig. 8. The stars are typical of the sample, and illustrate the level of agreement usually achieved. Clearly some of the differences in the Stokes *I* profiles result from small CS contributions to the real spectrum (e.g. HD 244604, lower-left panel). The remainder we attribute mainly to errors in the adopted atmospheric parameters and the detailed chemistry of the star. HD 34282 and HD 68695 are both instructive in this respect: a detailed examination of their spectra reveals underabundances of the Fe peak elements that dominate their spectra, while the abundance of oxygen appears to be solar. This suggests that these two stars represent further examples of HAeBe stars with λ Boo abundance patterns (Cowley et al. 2010; Folsom et al. 2012). In fact, one of these stars (HD 68695) was analysed by Folsom et al., who found it to exhibit clear λ Boo abundance peculiarities. From Fig. 7 we conclude that typically our spectrum synthesis approach is able to determine the expected longitudinal field error bar within ±20 per cent, although larger deviations sometimes occur for stars with strongly peculiar chemistry.

Examples of the remaining stars – those with profiles with significant CS contributions – are shown in Fig. 9. In these cases the magnetic diagnosis is highly uncertain, and often no reasonable diagnosis can be performed using the observed Stokes *I* profile. When we measure the longitudinal fields of the hybrid profiles of these objects, we find that while sometimes the error bars are reduced, sometimes they increase significantly. Examination of individual profiles reveals that often when the error bar derived by our method is significantly larger than that from the observed profile,

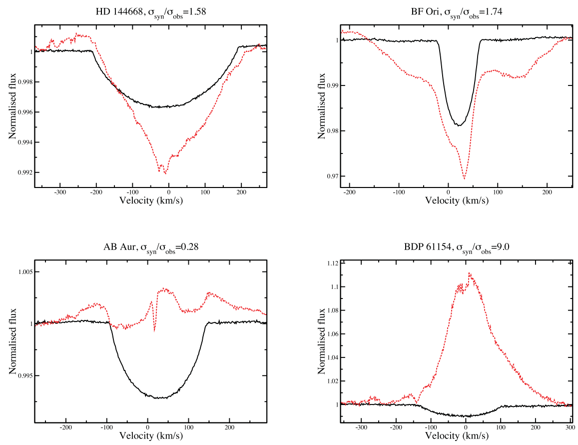

Figure 9. Illustrations of observed versus synthetic LSD Stokes *I* profiles for stars with profiles dominated by the circumstellar component. The black full line is the synthetic, and the red dashed line is the observed. Upper left: HD 144668. Upper right: BF Ori. Lower left: AB Aur. Lower right: BD+61 154.

it is because the observed profile is in strong emission or contains strong CS absorption, artificially increasing the magnitude of the equivalent width (e.g. BD+61 154, lower-right panel of Fig. 9, HD 144668 and BF Ori, upper panels of Fig. 9). On the other hand, partial infilling of the photospheric profile as a result of CS contributions may reduce the equivalent width, thereby increasing the error bar relative to that obtained from a synthetic profile (e.g. AB Aur, lower-left panel of Fig. 9). In some extreme cases, the infilling can produce an observed equivalent width very close to zero, resulting in a divergent longitudinal field and error bar (e.g. HD 50083, observed on 2008 April 3. Interestingly, the observation obtained on 2007 November 12 has much less infilling, and a much more realistic error bar).

The results we obtain from our hybrid analysis are very different from those that we would obtained using the clean masks derived for the profile analysis of Section 5.2. To illustrate, in Table 4 there are 44 measurements (corresponding to 19 stars) with 'hybrid' error bars smaller than 100 G. In contrast, analysis of the 'clean' profiles results in only 10 measurements smaller than 100 G. For some stars for which the raw and hybrid profiles yield quite good errors (a few tens of gauss), the clean profiles produce errors of hundreds of gauss. This confirms our view that in many cases, the line masks required to obtain a relatively pure photospheric profile for determining e.g. $v \sin i$ are not suitable to obtain profiles yielding the most realistic magnetic diagnosis.

Based on these experiments and examination of individual profiles, we conclude that our hybrid approach provides a useful way of determining the longitudinal magnetic field for a large and diverse sample of HAeBe stars, and that while inherent uncertainties exist in the determination of the longitudinal field using synthetic photospheric Stokes *I* profiles, those uncertainties (errors in atmospheric parameters, detailed chemistry) are better controlled and understood than the uncertainties associated with the determination of $\langle B_z \rangle$ using the observed Stokes *I* profiles. We therefore recommend the use of the hybrid determinations of $\langle B_z \rangle$ for characterization of the magnetic fields of individuals stars or samples of stars for which poorly understood contamination of Stokes *I* by CS environment is a problem.

In order to evaluate the impact of our choices of the masks on the $\langle B_z \rangle$ and their uncertainties, we have computed new LSD profiles of different stars of our sample with various masks of different temperature, gravity and abundance. We have then computed new values of $\langle B_z \rangle$ and compared them to those of Table 4. We selected stars in our sample of various spectral types and rotation velocities, and with small CS contribution. We changed the temperature within the error bars (Table 2), $\log g$ from 3.5 to 4.5, and the abundance at ±25 per cent. We find that $\langle B_z \rangle$ varies within the error bars in all cases. The uncertainties on $\langle B_z \rangle$ vary by a factor of <1 per cent when $\log g$ and the abundances are varied. When we change the temperatures, the uncertainties vary from 1 per cent (for large uncertainties of ∼800 G) to 10 per cent (for uncertainties lower than ∼100 G).

Of the 70 stars observed in our survey, 65 (93 per cent) show no direct evidence of a magnetic field. The derived characteristics of the longitudinal magnetic fields of the sample are summarized in Table 4. The magnetic geometries of the detected stars, as well as interpretation of the general magnetic properties of the sample from the distributions illustrated in Fig. 10, will be discussed in detail in Paper III.

7 CONCLUSIONS

This paper is the first of a series that presents the results of a high-resolution spectropolarimetric analysis of a sample of 70 Herbig Ae/Be stars. We carried out this analysis in order to address the problems of magnetism, angular momentum evolution and CS environment during the PMS phase of intermediate-mass stars.

We obtained 132 high-resolution Stokes *I* and *V* spectra of 70 HAeBe stars using the instruments ESPaDOnS at CFHT and Narval at TBL. In this paper, we have described the sample selection, the observations and their reduction, and the measurements that will comprise the basis of much of our following analysis. We have described the determination of fundamental parameters for each target.

(i) The published effective temperatures have been verified by a visual comparison of observed with synthetic spectra. For some stars, new determinations of $T_{\rm eff}$ are given here. In the case of a few stars with high-S/N observations weakly contaminated by CS material, we have redetermined their $T_{\rm eff}$ with an automatic procedure described here.

(ii) The luminosities have been estimated using the most reliable distance and photometric data that we could find in the literature.

(iii) The radius, mass and age have been determined by comparing the position of the stars in an HR diagram with PMS evolutionary tracks computed with CESAM. The ages have been measured from the birthline of BM01.

We discuss the LSD method that we have applied to each of our spectra, including the careful selection, editing and tuning of the LSD line masks. We describe the fitting of the LSD Stokes *I* profiles using a multicomponent model that yields the rotationally broadened photospheric profile (providing the projected rotational velocity and radial velocity for each observation) as well as CS emission and absorption components. The $v \sin i$ measurements are summarized in Table 2.

Finally, we detail the method that we used to confidently affirm that a star is magnetic. We diagnosed the longitudinal Zeeman effect via the measured circular polarization inside spectral lines. In this survey, five (out of 70) HAeBe stars have been confirmed

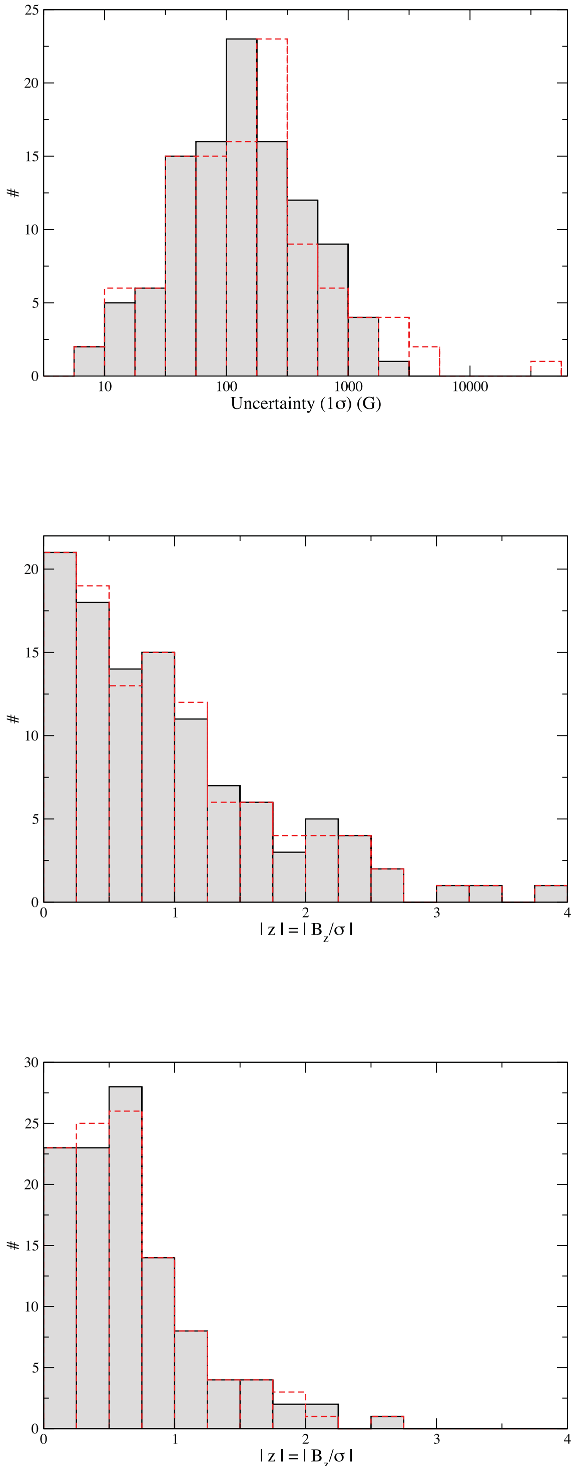

Figure 10. Final results for the longitudinal field uncertainties of the program stars. Upper panel: error bars from the hybrid and original LSD profiles. The black filled histogram corresponds to the hybrid profiles, while the dashed red unfilled histogram corresponds to the original profiles. Middle panel: detection significance $z = |\langle B_z \rangle / \sigma|$. Note that the three detections (i.e. $z \geq 3$) correspond to the magnetic HAeBe star LP Ori and to the suspected magnetic HAeBe star HD 35929. Both are sometimes detected in the *V* signatures of the LSD profiles and in $\langle B_z \rangle / \sigma$. Lower panel: same as the middle panel but for the *N* profiles. Note on one side the absence of detections (i.e. $z \leq 3$), and on the other side, the numerous values with *z* between 1 and 2, while by definition an *N* spectrum does not contain any signal.

to be magnetic (V380 Ori and HD 72106 reported by Wade et al. 2005; HD 190073 by Catala et al. 2007; HD 200775 by Alecian et al. 2008a; LP Ori by Petit et al. 2008). Four of them have been discovered within this program. One star (HD 35929) is reported here as a new suspected magnetic star. We also present the 'hybrid' method that we have adopted in order to obtain realistic quantitative measurements of the magnetic fields of the 65 non-magnetic stars. The results are reported in Tables 3 and 4.

As an appendix, we have also provided a detailed review of each star observed.

In three forthcoming papers we will present out analysis of the rotational properties of the sample (Paper II), the magnetic properties of the sample (Paper III) and the properties of the CS environment of the Herbig Ae/Be stars (Paper IV).

ACKNOWLEDGMENTS

We are very grateful to O. Kochukhov, who provided his BINMAG1 code. We thank Nikolai Piskunov, the referee, who led to important improvements in the paper. EA has been supported by the Marie Curie FP6 programme and the Centre National d'Etudes Spatiales (CNES). EA has also been supported by the Ministry of Higher Education and Research (MESR) and the Ministry of Foreign and European Affairs (MAEE), via the Hubert Curien Partnership (PHC) FAST (French-Australian Science & Technology). GAW and JDL acknowledge support from the Natural Science and Engineering Research Council of Canada (NSERC). GAW has also been supported by the DND Academic Research Programme (ARP). This research has made use of the SIMBAD data base and the VizieR catalogue access tool, operated at CDS, Strasbourg (France), and of NASA's Astrophysics Data System. SM and IW have been supported by the Commonwealth of Australia under the International Science Linkages programme.

REFERENCES

Abt H. A., 2009, AJ, 138, 28
Abt H. A., Morrell N. I., 1995, ApJS, 99, 135
Acke B., van den Ancker M. E., 2004, A&A, 426, 151
Acke B., Waelkens C., 2004, A&A, 427, 1009
Alecian E. et al., 2008a, MNRAS, 385, 391
Alecian E. et al., 2008b, A&A, 481, L99
Alecian E. et al., 2009a, in Neiner C., Zahn J.-P., eds, EAS Publications Series, Vol. 39, Magnetism in Herbig Ae/Be Stars and the Link to the Ap/Bp Stars. EDP Sciences, Les Ulis, p. 121
Alecian E. et al., 2009b, MNRAS, 400, 1250
Alecian E. et al., 2013, MNRAS, 429, 1027 (Paper II)
Alencar S. H. P., Melo C. H. F., Dullemond C. P., Andersen J., Batalha C., Vaz L. P. R., Mathieu R. D., 2003, A&A, 409, 1037
Alonso-Albi T., Fuente A., Bachiller R., Neri R., Planesas P., Testi L., Berné O., Joblin C., 2009, A&A, 497, 117
Andersen J., Lindgren H., Hazen M. L., Mayor M., 1989, A&A, 219, 142
Artymowicz P., 2000, Space Sci. Rev., 92, 69
Augereau J. C., Lagrange A. M., Mouillet D., Ménard F., 1999, A&A, 350, L51
Aveni A. F., Hunter J. H., 1972, AJ, 77, 17
Beals C. S., 1953, Publ. Dominion Astrophys. Obser. Victoria, 9, 1
Behrend R., Maeder A., 2001, A&A, 373, 190 (BM01)
Bernabei S. et al., 2009, A&A, 501, 279
Bernes C., 1977, A&AS, 29, 65
Beskrovnaya N. G. et al., 1999, A&A, 343, 163
Blaauw A., 1964, ARA&A, 2, 213

Boersma C., Peeters E., Martín-Hernández N. L., van der Wolk G., Verhoeff A. P., Tielens A. G. G. M., Waters L. B. F. M., Pel J. W., 2009, A&A, 502, 175
Böhm T., Catala C., 1994, A&A, 290, 167
Böhm T., Catala C., 1995, A&A, 301, 155
Bouret J.-C., Catala C., 1998, A&A, 340, 163
Bouret J.-C., Catala C., Simon T., 1997, A&A, 328, 606
Brown A. G. A., de Geus E. J., de Zeeuw P. T., 1994, A&A, 289, 101
Catala C., Czarny J., Felenbok P., Praderie F., 1986a, A&A, 154, 103
Catala C., Felenbok P., Czarny J., Talavera A., Boesgaard A. M., 1986b, ApJ, 308, 791
Catala C., Simon T., Praderie F., Talavera A., The P. S., Tjin A Djie H. R. E., 1989, A&A, 221, 273
Catala C., Böhm T., Donati J.-F., Semel M., 1993, A&A, 278, 187
Catala C., Donati J. F., Böhm T., Landstreet J., Henrichs H. F., 1999, A&A, 345, 884
Catala C. et al., 2007, A&A, 462, 293
Corcoran M., Ray T. P., 1998, A&A, 331, 147
Corporon P., Lagrange A.-M., 1999, A&AS, 136, 429
Coulson I. M., Walther D. M., Dent W. R. F., 1998, MNRAS, 296, 934
Cowley C. R., Hubrig S., González J. F., Savanov I., 2010, A&A, 523, A65
Crawford D. L., Barnes J. V., 1970, AJ, 75, 952
de Winter D., van den Ancker M. E., Maira A., Thé P. S., Djie H. R. E. T. A., Redondo I., Eiroa C., Molster F. J., 2001, A&A, 380, 609
de Zeeuw P. T., Hoogerwerf R., de Bruijne J. H. J., Brown A. G. A., Blaauw A., 1999, AJ, 117, 354
Deleuil M. et al., 2005, A&A, 429, 247
Dent W. R. F., Greaves J. S., Coulson I. M., 2005, MNRAS, 359, 663
Doering R. L., Meixner M., 2009, AJ, 138, 780
Dolan C. J., Mathieu R. D., 2001, AJ, 121, 2124
Donati J.-F., Semel M., Rees D. E., 1992, A&A, 265, 669
Donati J.-F., Semel M., Carter B. D., Rees D. E., Collier Cameron A., 1997, MNRAS, 291, 658
Donati J.-F. et al., 2003, MNRAS, 345, 1145
Doucet C., Pantin E., Lagage P. O., Dullemond C. P., 2006, A&A, 460, 117
Dunkin S. K., Crawford I. A., 1998, MNRAS, 298, 275
Eggen O. J., 1986, AJ, 92, 1074
Eiroa C. et al., 2001, A&A, 365, 110
Eisner J. A., Lane B. F., Hillenbrand L. A., Akeson R. L., Sargent A. I., 2004, ApJ, 613, 1049
Eisner J. A., Graham J. R., Akeson R. L., Najita J., 2009, ApJ, 692, 309
ESA, 1997, VizieR Online Data Catalog, 1239, 0
Fabricius C., Makarov V. V., 2000, A&A, 356, 141
Fernández D., Figueras F., Torra J., 2008, A&A, 480, 735
Finkenzeller U., 1985, A&A, 151, 340
Finkenzeller U., Mundt R., 1984, A&AS, 55, 109
Folsom C. P., Bagnulo S., Wade G. A., Alecian E., Landstreet J. D., Marsden S. C., Waite I. A., 2012, MNRAS, 422, 2072
Folsom C. P. et al., 2008, MNRAS, 391, 901
Fossati L., Ryabchikova T., Bagnulo S., Alecian E., Grunhut J., Kochukhov O., Wade G., 2009, A&A, 503, 945
Frémat Y., Neiner C., Hubert A., Floquet M., Zorec J., Janot-Pacheco E., Renan de Medeiros J., 2006, A&A, 451, 1053
Friedemann C., Reimann H., Guertler J., 1992, A&A, 255, 246
Getman K. V. et al., 2005, ApJS, 160, 319
Ghandour L., Strom S., Edwards S., Hillenbrand L., 1994, in The P. S., Perez M. R., van den Heuvel E. P. J., eds, ASP Conf. Ser. Vol. 62, The Nature and Evolutionary Status of Herbig Ae/Be Stars. Astron. Soc. Pac., San Francisco, p. 223
Grady C. A., Perez M. R., The P. S., 1993, A&A, 274, 847
Grady C. A., Sitko M. L., Russell R. W., Lynch D. K., Hanner M. S., Perez M. R., Bjorkman K. S., de Winter D., 2000b, Protostars and Planets IV, Univ. Arizona Press, Tucson, p. 613
Grady C. A. et al., 1996, A&AS, 120, 157
Grady C. A. et al., 2000a, ApJ, 544, 895
Gray D. F., 1992, The Observation and Analysis of Stellar Photospheres, 2nd edn. Cambridge Univ. Press, Cambridge, ISBN 0521403200
Gregorio-Hetem J., Lepine J. R. D., Quast G. R., Torres C. A. O., de La Reza R., 1992, AJ, 103, 549
Grinin V. P., Kozlova O. V., Natta A., Ilyin I., Tuominen I., Rostopchina A. N., Shakhovskoy D. N., 2001, A&A, 379, 482
Guetter H. H., 1976, AJ, 81, 537
Guetter H. H., 1979, AJ, 84, 1846
Guetter H. H., 1981, AJ, 86, 1057
Guimarães M. M., Alencar S. H. P., Corradi W. J. B., Vieira S. L. A., 2006, A&A, 457, 581
Günther H. M., Schmitt J. H. M. M., 2009, A&A, 494, 1041
Harvey P. M. et al., 2008, ApJ, 680, 495
Herbig G. H., 1960, ApJS, 4, 337
Herbig G. H., Bell K. R., 1988, Lick Obs. Bull., No. 1111
Herbst W., 1975, AJ, 80, 683
Herbst W., Shevchenko V. S., 1999, AJ, 118, 1043
Herbst W., Warner J. W., Miller D. P., Herzog A., 1982, AJ, 87, 98
Hernández J., Calvet N., Briceño C., Hartmann L., Berlind P., 2004, AJ, 127, 1682
Hernández J., Calvet N., Hartmann L., Briceño C., Sicilia-Aguilar A., Berlind P., 2005, AJ, 129, 856
Hill P. W., 1970, MNRAS, 150, 23
Hillenbrand L. A., Strom S. E., Vrba F. J., Keene J., 1992, ApJ, 397, 613
Hillenbrand L. A., Strom S. E., Calvet N., Merrill K. M., Gatley I., Makidon R. B., Meyer M. R., Skrutskie M. F., 1998, AJ, 116, 1816
Houk N., 1982, Michigan Catalogue of Two-dimensional Spectral Types for the HD Stars, Vol. 3: Declinations −40 deg to −26 deg. Department of Astronomy, University of Michigan, Ann Arbor, MI, USA
Houk N., 1994, VizieR Online Data Catalog, 3080, 0
Hubeny I., 1988, Comput. Phys. Commun., 52, 103
Hubeny I., Lanz T., 1992, A&A, 262, 501
Hubeny I., Lanz T., 1995, ApJ, 439, 875
Hubrig S., Schöller M., Yudin R. V., 2004, A&A, 428, L1
Hubrig S. et al., 2009, A&A, 502, 283
Hughes A. M., Wilner D. J., Kamp I., Hogerheijde M. R., 2008, ApJ, 681, 626
Hussain G. A. J. et al., 2009, MNRAS, 398, 189
Høg E., Kuzmin A., Bastian U., Fabricius C., Kuimov K., Lindegren L., Makarov V. V., Roeser S., 1998, A&A, 335, L65
Høg E. et al., 2000, A&A, 355, L27
Jenniskens P., Desert F., 1994, A&AS, 106, 39
Johnson H. M., 1965, ApJ, 142, 964
Jordi C., Trullols E., Galadi-Enriquez D., 1996, A&A, 312, 499
Juhász A., Prusti T., Ábrahám P., Dullemond C. P., 2007, MNRAS, 374, 1242
Jura M., Malkan M., White R., Telesco C., Pina R., Fisher R. S., 1998, ApJ, 505, 897
Keller L. D. et al., 2008, ApJ, 684, 411
Kenyon S. J., Hartmann L., 1995, ApJS, 101, 117
Kharchenko N. V., Piskunov A. E., Röser S., Schilbach E., Scholz R., 2004, Astron. Nachr., 325, 740
Kharchenko N. V., Piskunov A. E., Röser S., Schilbach E., Scholz R., 2005, A&A, 438, 1163
Kholopov P. N., 1959, SvA, 3, 291
Kochukhov O. P., 2007, in Romanyuk I. I., Kudryavtsev D. O., Neizvestnaya O. M., Shapoval V. M., eds, Physics of Magnetic Stars. p. 109
Kovalchuk G. U., Pugach A. F., 1997, A&A, 325, 1077
Kraus S., Preibisch T., Ohnaka K., 2008, ApJ, 676, 490
Kun M., 1998, ApJS, 115, 59
Kun M., Vinkó J., Szabados L., 2000, MNRAS, 319, 777
Kupka F., Piskunov N., Ryabchikova T. A., Stempels H. C., Weiss W. W., 1999, A&AS, 138, 119

Kurucz R., 1993, Opacities for Stellar Atmospheres: [−3.5],[−4.0],[−4.5]. Kurucz CD-ROM, No. 7. Smithsonian Astrophysical Observatory, Cambridge, MA
Landstreet J. D., 1982, ApJ, 258, 639
Larson R. B., 1972, MNRAS, 157, 121
Levato H., Abt H. A., 1976, PASP, 88, 712
Levreault R. M., 1985, PhD thesis, Texas University, Austin
Lynds B. T., 1962, ApJS, 7, 1
Magakian T. Y., 2003, A&A, 399, 141
Malfait K., Bogaert E., Waelkens C., 1998, A&A, 331, 211
Mannings V., Barlow M. J., 1998, ApJ, 497, 330
Mannings V., Sargent A. I., 1997, ApJ, 490, 792
Manoj P., Maheswar G., Bhatt H. C., 2002, MNRAS, 334, 419
Manset N., Bastien P., Bertout C., 2005, AJ, 129, 480
Marconi M., Ripepi V., Alcalá J. M., Covino E., Palla F., Terranegra L., 2000, A&A, 355, L35
Martayan C., Floquet M., Hubert A. M., Neiner C., Frémat Y., Baade D., Fabregat J., 2008, A&A, 489, 459
Mathys G., 1991, A&AS, 89, 121
Merín B., Montesinos B., Eiroa C., Solano E., Mora A., 2004, A&A, 419, 301
Michaud G., 1970, ApJ, 160, 641
Michaud G., Charland Y., Megessier C., 1981, A&A, 103, 244
Miroshnichenko A. S., Gray R. O., Vieira S. L. A., Kuratov K. S., Bergner Y. K., 1999a, A&A, 347, 137
Miroshnichenko A., Ivezić Ž., Vinković D., Elitzur M., 1999b, ApJ, 520, L115
Miroshnichenko A. S., Bjorkman K. S., Chentsov E. L., Klochkova V. G., Gray R. O., García-Lario P., Perea Calderón J. V., 2001, A&A, 377, 854
Miroshnichenko A. S., Gray R. O., Klochkova V. G., Bjorkman K. S., Kuratov K. S., 2004, A&A, 427, 937
Montesinos B., Eiroa C., Mora A., Merín B., 2009, A&A, 495, 901
Mora A. et al., 2001, A&A, 378, 116
Mora A., Natta A., Eiroa C., Grady C. A., de Winter D., Davies J. K., Ferlet R., Harris A. W., 2002, A&A, 393, 259
Mora A. et al., 2004, A&A, 419, 225
Morel P., 1997, A&AS, 124, 597
Müller A., van den Ancker M. E., Launhardt R., Pott J. U., Fedele D., Henning T., 2011, A&A, 530, A85
Murdin P., Penston M. V., 1977, MNRAS, 181, 657
Natta A., Grinin V. P., Tambovtseva L. V., 2000, ApJ, 542, 421
Mimes CollaborationNeiner C., Alecian E., Briquet M., Floquet M., Frémat Y., Martayan C., Thizy O., 2012, A&A, 537, A148
Nesterov V. V., Kuzmin A. V., Ashimbaeva N. T., Volchkov A. A., Röser S., Bastian U., 1995, A&AS, 110, 367
Norberg P., Maeder A., 2000, A&A, 359, 1025 (NM00)
Oliver R. J., Masheder M. R. W., Thaddeus P., 1996, A&A, 315, 578
Oudmaijer R. D., van der Veen W. E. C. J., Waters L. B. F. M., Trams N. R., Waelkens C., Engelsman E., 1992, A&AS, 96, 625
Oudmaijer R. D. et al., 2001, A&A, 379, 564
Palla F., Stahler S. W., 1990, ApJ, 360, L47
Palla F., Stahler S. W., 1991, ApJ, 375, 288
Palla F., Stahler S. W., 1992, ApJ, 392, 667
Palla F., Stahler S. W., 1993, ApJ, 418, 414 (PS93)
Paunzen E., Duffee B., Heiter U., Kuschnig R., Weiss W. W., 2001, A&A, 373, 625
Pèrez M. R., Imhoff C. L., Thè P. S., 1991, BAAS, 23, 1374
Perryman M. A. C., ESA, eds, 1997, ESA-SP 1200, The *Hipparcos* and Tycho Catalogues. ESA, Noordwijk
Petit P. et al., 2004, MNRAS, 348, 1175
Petit V., Wade G. A., Drissen L., Montmerle T., Alecian E., 2008, MNRAS, 387, L23
Piskunov N. E., 1992, in Glagolevskij Yu. V., Romanyuk I. I., eds, Stellar Magnetism synth – a Code for Rapid Spectral Synthesis Proc. Int. Meeting Physics and Evolution of Stars. NAUKA, St Petersburg, p. 92
Piskunov N. E., Kupka F., Ryabchikova T. A., Weiss W. W., Jeffery C. S., 1995, A&AS, 112, 525
Pontoppidan K. M., Dullemond C. P., Blake G. A., Boogert A. C. A., van Dishoeck E. F., Evans II N. J., Kessler-Silacci J., Lahuis F., 2007, ApJ, 656, 980
Praderie F., Catala C., Simon T., Boesgaard A. M., 1986, ApJ, 303, 311
Preibisch T., Mamajek E., 2008, in Reipurth B., ed., Handbook of Star-Forming Regions, Vol. II. Astron. Soc. Pac., San Francisco, p. 235
Preibisch T., Kraus S., Driebe T., van Boekel R., Weigelt G., 2006, A&A, 458, 235
Press W. H., Teukolsky S. A., Vetterling W. T., Flannery B. P., 1992, in Press W. H., Teukolsky S. A., Vetterling W. T., Flannery B. P., eds, Numerical Recipes in C. The Art of Scientific Computing. Cambridge Univ. Press, Cambridge
Prusti T., Natta A., Palla F., 1994, A&A, 292, 593
Pugach A. F., Kovalchuk G. U., 1986, Astron. Nachr., 307, 13
Reid M. J. et al., 2009, ApJ, 700, 137
Rostopchina A. N., Grinin V. P., Shakhovskoi D. N., Thé P. S., Minikulov N. K., 2000, Astron. Rep., 44, 365
Ryabchikova T., Piskunov N., Savanov I., Kupka F., Malanushenko V., 1999, A&A, 343, 229
Saffe C., Gómez M., Pintado O., González E., 2008, A&A, 490, 297
Sahu M. S., Blades J. C., He L., Hartmann D., Barlow M. J., Crawford I. A., 1998, ApJ, 504, 522
Sandqvist A., Lindroos K. P., 1976, A&A, 53, 179
Sartori M. J., Gregorio-Hetem J., Rodrigues C. V., Hetem A., Batalha C., 2010, AJ, 139, 27
Semel M., 1989, A&A, 225, 456
Semel M., Donati J.-F., Rees D. E., 1993, A&A, 278, 231
Shakhovskoi D. N., Rostopchina A. N., Grinin V. P., Minikulov N. K., 2003, Astron. Rep., 47, 301
Shevchenko V. S., Yakubov S. D., 1989, SvA, 33, 370
Shevchenko V. S., Ibragimov M. A., Chenysheva T. L., 1991, SvA, 35, 229
Shevchenko V. S., Ezhkova O. V., Ibrahimov M. A., van den Ancker M. E., Tjin A Djie H. R. E., 1999, MNRAS, 310, 210
Shorlin S. L. S., Wade G. A., Donati J.-F., Landstreet J. D., Petit P., Sigut T. A. A., Strasser S., 2002, A&A, 392, 637
Shultz M. et al., 2012, ApJ, 750, 2
Silvester J. et al., 2009, MNRAS, 398, 1505
Straižys V., Černis K., Bartašiūte S., 1996, Balt. Astron., 5, 125
Stępień K., 2000, A&A, 353, 227
Strom S. E., Strom K. M., Yost J., Carrasco L., Grasdalen G., 1972, ApJ, 173, 353
Sylvester R. J., Skinner C. J., Barlow M. J., Mannings V., 1996, MNRAS, 279, 915
Testa P., Huenemoerder D. P., Schulz N. S., Ishibashi K., 2008, ApJ, 687, 579
Thé P. S., Cuypers H., Tjin A Djie H. R. E., Felenbok P., 1985a, A&A, 149, 429
Thé P. S., Tjin A Djie H. R. E., Catala C., Praderie F., Felenbok P., 1985b, The Messenger, 41, 8
Thé P. S., de Winter D., Perez M. R., 1994, A&AS, 104, 315
Tian K. P., van Leeuwen F., Zhao J. L., Su C. G., 1996, A&AS, 118, 503
Tjin A Djie H. R. E., The P. S., Andersen J., Nordstrom B., Finkenzeller U., Jankovics I., 1989, A&AS, 78, 1
van den Ancker M. E., The P. S., de Winter D., 1996, A&A, 309, 809
van den Ancker M. E., de Winter D., Tjin A Djie H. R. E., 1998, A&A, 330, 145
van den Bergh S., 1966a, AJ, 71, 990
van den Bergh S., 1966b, AJ, 71, 990
van Leeuwen F., 2007, A&A, 474, 653
Vieira S. L. A., Corradi W. J. B., Alencar S. H. P., Mendes L. T. S., Torres C. A. O., Quast G. R., Guimarães M. M., da Silva L., 2003, AJ, 126, 2971
Wade G. A., Donati J.-F., Landstreet J. D., Shorlin S. L. S., 2000, MNRAS, 313, 851
Wade G. A., Bagnulo S., Drouin D., Landstreet J. D., Monin D., 2007, MNRAS, 376, 1145
Wade G. A. et al., 2005, A&A, 442, L31
Wahhaj Z., Koerner D. W., Sargent A. I., 2007, ApJ, 661, 368
Walker M. F., 1959, ApJ, 130, 57

Wang S., Looney L. W., Brandner W., Close L. M., 2008, ApJ, 673, 315
Warren W. H. Jr, Hesser J. E., 1977, ApJS, 34, 115
Warren W. H. Jr, Hesser J. E., 1978, ApJS, 36, 497
Weinberger A. J., Becklin E. E., Schneider G., Smith B. A., Lowrance P. J., Silverstone M. D., Zuckerman B., Terrile R. J., 1999, ApJ, 525, L53
Weinberger A. J., Rich R. M., Becklin E. E., Zuckerman B., Matthews K., 2000, ApJ, 544, 937
Wheelwright H. E., Oudmaijer R. D., Goodwin S. P., 2010, MNRAS, 401, 1199
Wolff S. C., Strom S. E., Hillenbrand L. A., 2004, ApJ, 601, 979

APPENDIX A: ANALYSIS OF INDIVIDUAL STARS

This appendix describes the approach that has been followed in order to determine the $v \sin i$ of all the stars of our sample, and the fundamental parameters (luminosity, effective temperature and surface gravity) required to estimate the masses and ages of the stars, which will be used in the statistical analysis described in Paper II. The basic procedure we have followed has been to first check that the effective temperature found in the literature corresponds to our data, and modify it if necessary. Then we have computed the LSD profiles for most of the data, using masks of appropriate temperature and gravity for each star, and fitted them (see Section 5). Sometimes it was necessary to add one or more Gaussian functions to the photospheric rotational velocity broadening function in order to obtain a better fit, and hence a more accurate value of the $v \sin i$. This paper does not aim to propose a physical origin of these Gaussian functions. Most of them are assumed to have a CS origin. However, a more detailed analysis of the non-photospheric spectral features observed in the spectra (and in the LSD profiles) of our sample will be presented in a forthcoming paper. This appendix summarizes only the information required to fully understand the method that we applied to determine the $v \sin i$ of the stars.

For each of the stars we compared the observed normalized spectra with a grid of synthetic spectra, in order to check the published values and estimate new ones if required. As described above, these spectra assume solar chemical composition. In most cases the effective temperature could be estimated from this comparison, but not the surface gravity, due to imperfect continuum normalization of individual echelle orders and/or CS contamination. Therefore, unless specified, we used by default a surface gravity $\log g = 4.0$ (CGS) (see Section 4.1). In order to better understand the shape of the LSD profiles and the choice of the adopted mask, a description of the non-photospheric features has been added for each star. In these descriptions, the Balmer profile emission types that are sometimes mentioned have been classified according to the system of Beals (1953).

For each one of the stars, a short discussion has also been added to support their PMS nature, and therefore to justify their membership to our sample. The references of the photometric data and the distances used to derive the luminosity are also detailed. In the cases of stars that are members of the Orion OB 1 association, the distance adopted is the weighted mean of the distances of the six subgroups described by Brown et al. (1994).

Finally, apart from LP Ori, for which we obtained more data since its magnetic detection reported in Petit et al. (2008), this appendix concerns only the stars that have not been detected as magnetic. For the magnetic stars we refer the reader to the following papers: Catala et al. (2007), Alecian et al. (2008a), Folsom et al. (2008), Alecian et al. (2009b) and Paper IV.

A1 BD−06 1259 (= BF Ori)

BF Ori is a member of the subgroup c of the Ori OB 1 association (Warren & Hesser 1978), at a distance of 375 pc (Brown et al. 1994). It belongs to the UXOR subclass of HAeBe objects (hereafter UXOR stars; Mora et al. 2004), whose the prototype is UX Ori (see Section A61 in the online version of this paper). These stars are strong photometric variables. For the same reasons as for UX Ori, we used the *Hipparcos* photometric data (Perryman & ESA 1997) at maximum brightness ($V_{\mathrm{T}} = 7.81$ mag, $B_{\mathrm{T}} = 7.85$ mag, in the Tycho system), and converted them to the Johnson system (see the method in Section A61 in the online version of this paper). We find $V = 7.85$ mag and $(B - V) = -0.028$ mag, values that have been adopted to derive the luminosity of the star. BF Ori displays strong near-IR excess, very likely due to the presence of an optically thick CS accretion disc (Hillenbrand et al. 1992).

The spectrum of BF Ori is very complex, highly variable and similar to other UXOR stars. In the 2005 February spectrum, we can distinguish two classes of spectral lines among the metals. The first class consists of strong and broad CS absorption features at the positions of the predicted strong photospheric lines. These lines are still observed in the 2009 March spectrum, with different shapes and increased depth. The second class of lines concerns the predicted weak lines of the spectrum, which show a photospheric component on which is superimposed a narrower CS absorption. In our 2009 spectrum these lines show only photospheric components. As with other UXOR stars, these transient absorption features are assumed to come from gaseous clouds in the disc of the star (see Section A61 in the online version of this paper).

The Balmer lines from Hδ to Hβ show strong absorption components superimposed on the cores of the photospheric lines, with weak emission in the wings of the absorption component. The amplitudes of these features increase with wavelength, and their shape has changed between our two observations. Hα is in emission with a double-peaked profile of type VI and a strong central absorption that goes below the continuum. The amplitude of the emission doubled between 2005 and 2009. The Ca II K line, the He I lines at 5875, 6678 and 7065 Å, and the O I 7775 Å and O I 8446 Å triplets display very strong (stronger than predicted) absorption profiles. The three IR Ca II lines at 8498, 8542 and 8662 Å (hereafter the Ca II IR triplet) show strong and broad emission profiles superimposed on the three photospheric absorption lines. The Paschen lines seem also to be slightly contaminated with CS emission.

The wings of the Balmer lines are consistent with the temperature and surface gravity determination of Mora et al. (2004, $T_{\mathrm{eff}} = 8750 \pm 250$ K, $\log g = 4.0 \pm 0.5$). We have cleaned the Kurucz mask by rejecting as many contaminated lines as possible. The resulting LSD profile for 2009 shows only a photospheric component. However, the 2005 profile still shows a photospheric line with a superimposed CS absorption component. We first tried to fit both observations simultaneously using the following model: a photospheric profile + a Gaussian function in absorption for the 2005 profile, and only a photospheric profile for the 2009 observation. However, we found that fitting the 2009 profile only resulted in a more accurate value of $v \sin i$. We therefore adopted this value. The resulting fit is shown in Fig. A1.

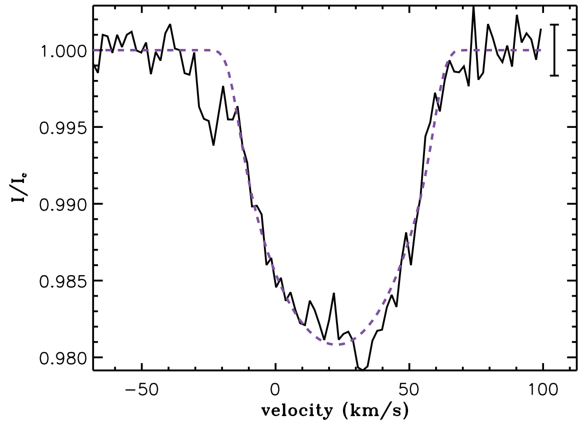

Figure A1. The LSD *I* profile of the 2009 March observation of BD−06 1259 = BF Ori (black full line), superimposed with its best fit (purple dashed line).

SUPPORTING INFORMATION

Additional Supporting Information may be found in the online version of this article:

Appendix A: Analysis of individual stars (http://mnras.oxfordjournals.org/lookup/suppl/doi:10.1093/mnras/sts383/-/DC1).

Please note: Oxford University Press are not responsible for the content or functionality of any supporting materials supplied by the authors. Any queries (other than missing material) should be directed to the corresponding author for the article.

This paper has been typeset from a TEX/LATEX file prepared by the author.